Research Article

Biophysical Characterization of Recurrent ErbB2 Missense Mutations Reveals Alterations in Receptor Organization and Membrane Dynamics

Tayde Gabriela Serrano Cano [1], Atena Yasari [2], Ingrid Hartl [2], Irene Tiemann-Boege [2], and Peter Nagy [1,*]

*1 - **Department of Biophysics and Cell Biology,** Faculty of Medicine, University of Debrecen, Debrecen, Hungary*
*2 - **Institute of Biophysics,** Johannes Kepler University, Linz, Austria*

***Correspondence to Peter Nagy:** nagyp@med.unideb.hu (P. Nagy)*
https://doi.org/10.1016/j.jmb.2026.169770
Edited by Lutz Schmitt

Abstract

The purpose of this study was to characterize three recurrent, cancer-associated missense mutations in ErbB2, R143Q, R678Q, and V842I, located in the extracellular, juxtamembrane and kinase domains, respectively, to determine how single amino acid substitutions affect receptor organization and dynamics. Using confocal microscopy, Förster resonance energy transfer (FRET) and fluorescence recovery after photobleaching (FRAP), we assessed homo- and heteroassociation, lateral diffusion and tyrosine phosphorylation of ErbB2 cancer-associated variants either alone or co-expressed with EGFR. The only individual biophysical property that differentiated the mutation-activated ErbB2 variants from the wild-type was an accelerated diffusion in the absence of EGFR coexpression. Correlative analysis of the biophysical properties of ErbB2 revealed that ErbB2-activating mutations, including the cancer-associated R143Q, R678Q and V842I mutations, may promote a pre-dimerized receptor state associated with accelerated lateral mobility, but without full-scale activation implied by the lack of growth factor-independent tyrosine phosphorylation. The faster mobility of mutation-activated ErbB2 contrasted with the EGF-induced slowing down of its lateral diffusion. In summary, single amino acid substitutions across ErbB2 domains may modulate receptor dynamics, organization, and responsiveness.

Introduction

The ErbB family of receptor tyrosine kinases is one of the most extensively studied transmembrane signaling systems, with well-established roles in human physiology and disease. Its founding member, the epidermal growth factor receptor (EGFR/ErbB1), is a typical receptor activated by a wide range of EGF-like ligands [1]. It shares significant sequence homology with the three other members of the family, ErbB2-4 [2]. Whereas neuregulins activate ErbB3 and ErbB4 [3], ErbB2 is unique. It lacks a known ligand and mainly acts as a ligand-independent co-receptor, forming heterodimers with other ErbB proteins to enhance signaling output [4–6].

Structural studies have provided detailed insights into the molecular basis of both ligand-induced activation and ligand-independent co-receptor function. Crystallographic analyses showed that EGFR, ErbB3, and ErbB4 adopt a closed conformation in the absence of ligand, while ligand binding stabilizes an extended extracellular structure with the dimerization arm exposed [7]. By contrast, the ectodomain of ErbB2 adopts a pre-extended conformation, with its dimerization arm constitutively exposed, and autoinhibitory intramolecular interactions preventing uncontrolled

activation [8,9]. EGF-stabilized extracellular domain homodimers of EGFR are symmetric [10]. While asymmetric homodimers of EGFR induced by other ligands may seem to be the exception [11], asymmetry is the rule for heterodimers involving the ErbB2 extracellular domain [12,13]. Live-cell imaging showed that EGF stimulation reduces EGFR diffusion [14,15] while ErbB2 mobility remains mostly constant, highlighting the stability of ErbB2-containing heterodimers [12]. ErbB2 expression increases the ligand-binding affinity of partner receptors, reduces their lysosomal degradation and prolongs their signaling activity [16,17].

Moreover, at high expression levels, ErbB2 can form homodimers and large clusters. These supramolecular assemblies organize receptors into structures that both limit and improve signaling based on their conformational state [6,12,18,19]. Recent super-resolution analyses have demonstrated that therapeutic interventions, like antibody binding, can disrupt ErbB2 nanoscale clustering. This highlights the sensitivity of membrane organization to external or structural changes [20].

Dimerization of the extracellular domain is relayed through the membrane, resulting in asymmetric dimerization and activation of the kinase domains, with the activator kinase turning on the other kinase, which is in the receiver conformation [21]. More recently, the formation of asymmetric kinase domain dimers has also been observed for ErbB heterodimers. The ErbB3 kinase domain with impaired activity has been shown to play the activator role to activate the ErbB2 kinase allosterically [22]. A strict sequential activation model has been suggested for the EGFR/ErbB2 heterodimer with ligand-bound EGFR always assuming the receiver role first [23], while others replace this strict sequence with a preference of different ErbB kinase domains for adopting the receiver role [24].

Additionally, membrane characteristics like lipid composition, curvature, and dipole potential affect receptor clustering and conformational changes [25–27]. Moreover, transmembrane proteins undergo lateral diffusion, which links their mobility to activation state and oligomerization. Activation often coincides with increased turnover and cytoskeleton-mediated transport, whereas clustering or oligomerization restricts diffusion through steric and cytoskeletal restrictions [14,15,28–30]. Dimerization, lateral mobility, and phosphorylation collectively shape the organization and movement of ErbB2 at the plasma membrane.

While gene amplification is the most recognized form of ErbB2 dysregulation, occurring in about 30% of breast cancers and linked to a poor prognosis [31,32], it is now clear that missense mutations also occur frequently across multiple cancer types [33–35]. Amplification and mutations both disturb receptor behavior. Amplification alters receptor abundance and clustering, while missense mutations can directly reshape conformation, dimerization propensity, diffusion dynamics, and phosphorylation patterns of individual receptor molecules [36]. Recent research has shown that missense mutations can act as oncogenic drivers [37] or passenger mutations [38], highlighting the need for detailed, mutation-specific characterization. Importantly, some mutations are found with relatively high frequency in patient cohorts, indicating that they may confer structural or regulatory changes relevant to tumor biology [39,40].

Among the numerous missense mutations in ErbB2, V842I, R143Q, and R678Q are among the most common ErbB2 variants identified in patient datasets [41,42]. V842I, a recurrent mutation in the kinase domain, is associated with increased activity [43]. R678Q, located in the juxtamembrane region, is frequently observed in various tumor types and may impact the interaction between the transmembrane and kinase domains [37,44,45]. R143Q, located in the extracellular domain, is less characterized, but due to its localization, it could impact folding stability or dimerization interactions [46,47].

In this study, we investigate the effect of these three missense mutations on the behavior of ErbB2 at the plasma membrane. By comparing V842I, R143Q, and R678Q with wild-type ErbB2, we established a biophysical framework that would help us understand how structural changes in different domains influence receptor organization and dynamics. Rather than directly connecting these effects to function or treatment, this work highlights the membrane-level impacts of individual missense mutations.

Methods

Cells plasmids and antibodies

Chinese hamster ovary (CHO) cells were obtained from the American Type Culture Collection (Manassas, VA) and cultured according to their specifications. The constructs expressing mutant ErbB2 were prepared as previously described [42]. The missense and nonsense mutations in the ErbB2 variants are shown in Figure 1. ErbB2-expressing CHO cells were generated by transient transfection of the wild-type or one of the mutant ErbB2-pcDNA3.1 plasmids using Lipofectamine® 2000 (Thermo Scientific, Waltham, MA). ErbB2 and EGF receptor-coexpressing CHO cells were generated by double transfection in a 1:1 ratio by one of the ErbB2 plasmids and human EGFR cloned into pcDNA3 (from Donna Arndt-Jovin, Max Planck Institute for Multidisciplinary Sciences, Göttingen, Germany) [48]. We used Alexa Fluor 564-trastuzumab and Alexa Fluor 647-trastuzumab for labeling ErbB2. Trastuzumab, marketed under the name of Trazimera, was obtained from Pfizer as a lyophilized powder intended for

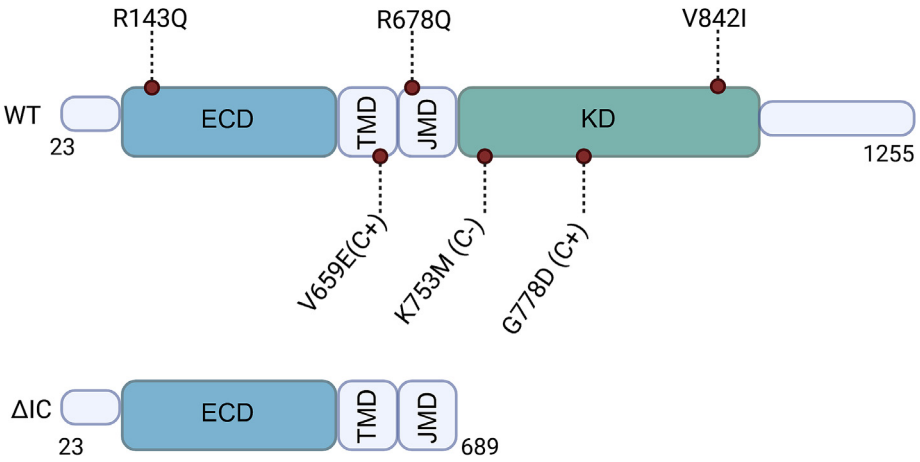

Figure 1. Schematic representation of full-length and the truncated (ΔIC) ErbB2 variants. The diagram illustrates the organization of the ErbB2 receptor, including the extracellular domain (ECD), the transmembrane domain (TMD), the juxtamembrane domain (JMD), and the tyrosine kinase domain (KD). The missense mutations analyzed are indicated: R143Q in the ECD, V959E (positive control, constitutively active) in the TMD, R678Q in the JMD, while K753M (negative control, kinase inactive), G778D (positive control, kinase active) and V842I are located in the KD. The mutant ΔIC, truncated at amino acid 689, lacks the intracellular domain and acts as a negative control (figure created in BioRender.com).

preparation of infusion for human use. The lyophilized powder containing 150 mg antibody, L-His, L-His hydrochloride monohydrate, saccharose and polyoxyethylene sorbitan monolaurate, was dissolved in PBS at a final trastuzumab concentration of 20 mg/mL. The antibody was labeled with Alexa Fluor 564 (A-20002, Thermo Scientific) and Alexa Fluor 647 (A-20006, Thermo Scientific) fluorescent dyes using their N-hydroxysuccinimidyl ester derivatives. Briefly, the antibody to be labeled was dissolved at a concentration of 2 mg/mL in a total volume of 750 μL in PBS supplemented with 75 μL of 1 M carbonate buffer. Depending on the degree of labeling to be achieved, 3–10 μL of the N-Hydroxysuccinimide derivative of the dye was added to the mixture followed by a 1-hour incubation at 25°C under constant agitation. Unreacted dye was removed by passing the reaction mixture through a Sephadex G-50 column (Sigma-Aldrich, GE17-0043-02) removing molecules smaller than ~30 kDa from the mixture. The degree of labeling was determined by spectrophotometry. The absorbance of the labeled antibody stock was measured at two wavelengths corresponding to the absorption maximum of the dye and to the absorption of amino acids in the UV range (280 nm):

$$A(\lambda_{dye}) = A_{dye}(\lambda_{dye}) = \varepsilon_{dye}\, c_{dye,M}\, L \tag{1}$$

$$A(280) = A_{IgG}(280) + A_{dye}(280) = \varepsilon_{IgG}\, c_{IgG,M}\, L + A_{dye}(\lambda_{dye})\, CF \tag{2}$$

where A is the absorbance of the species specified in the subscript measured at a wavelength specified in parentheses. ε_{IgG} is the molar absorption coefficient of the antibody at 280 nm and ε_{dye} is the molar absorption coefficient of the dye at its absorption maximum. $c_{dye,M}$ and $c_{IgG,M}$ are the molar concentrations of the dye and the antibody, respectively, L is the optical path length in cm and CF is a correction factor specifying the relative absorption of the dye at 280 nm compared to its absorption at its absorption maximum. These correction factors are available from the manufacturer or can be determined by measuring the absorption spectrum of the free dye. The molar concentrations of the dye and the antibody were determined from the equations above:

$$c_{IgG,M} = \frac{A(280) - A_{dye}(\lambda_{dye})\, CF}{\varepsilon_{IgG}\, L},\ c_{dye,M} = \frac{A_{dye}(\lambda_{dye})}{\varepsilon_{dye} L} \tag{3}$$

The degree of labeling is the ratio of the two molar concentrations:

$$DOL = \frac{c_{dye,M}}{c_{IgG,M}} \tag{4}$$

Trace amounts of unreacted dye, as well as residual amino acid additive conjugated to fluorescent dyes, may remain in the stock solutions, but they do not interfere with the microscopic measurements because only the fluorescent antibodies bound to their antigen contribute to the measured signals due to extensive washing after labeling of cells.

In order to quantify phosphotyrosines, monoclonal antibody PY99 (sc-7020, Santa Cruz Biotechnology, Dallas, TX) was used, while ErbB2 phosphorylated at Tyr1248 and EGFR phosphorylated at sites Tyr1048 and Tyr1173 was quantified by mouse monoclonal antibodies Ab18 (MS-1072, Thermo Scientific), EM-1 (11–575, ExBio) and 1H12 (2236, Cell Signaling), respectively, followed by staining with Alexa

Fluor647-conjugated goat anti-mouse IgG (A21236, Thermo Scientific).

Transfection and staining of cells for measuring protein clustering and lateral diffusion

CHO cells transiently transfected with wild-type or one of the mutant ErbB2 versions were stained with a mixture of Alexa Fluor564-trastuzumab and Alexa Fluor647-trastuzumab followed by measuring ErbB2 homoclustering using intensity-based Förster resonance energy transfer (FRET) between the donor and the acceptor on a Zeiss LSM880 confocal laser scanning microscope (Carl Zeiss AG, Oberkochen, Germany). For measuring heterodimerization of EGF receptor and ErbB2, CHO cells were double-transfected with plasmids coding for wild-type EGF receptor and one of the ErbB2 variants. Twenty-four hours after transfection, cells underwent overnight serum starvation in medium containing 0.1% serum. For measuring EGFR-ErbB2 heteroassociation under unstimulated conditions, cells were labeled with a mixture of TAMRA-EGF (50 nM, E3481, ThermoFisher Scientific) and AlexaFluor647-trastuzumab (20 μg/mL) for 20 min on ice followed by washing and fixation in 1% formaldehyde for 20 min on ice. Since the cells were kept strictly on ice throughout the whole procedure, TAMRA-EGF did not result in their stimulation. For measuring heteroassociation between EGFR and ErbB2 in EGF-stimulated samples, cells were labeled by 50 nM TAMRA-EGF for 20 min on ice followed by incubating the samples for 10 min at 37°C to allow EGF to stimulate the cells. Afterwards, these samples were labeled by 20 μg/mL AlexaFluor647-trastuzumab for 20 min on ice followed by washing and fixation. In order to measure lateral mobility, cells were single or double-transfected as described above, and cells were serum-starved overnight in two days after transfection. Unlabeled EGF at a concentration of 50 nM was added to the cells on the thermostated stage of the microscope at 37°C for 10 min followed by measuring the lateral mobility of ErbB2 both in these EGF-stimulated and the unstimulated cells using fluorescence recovery after photobleaching (FRAP) based on the GFP fluorescence of the ErbB2 constructs.

Measurement of protein–protein interactions using FRET

Images were acquired with a Zeiss LSM 880 confocal microscope (Carl Zeiss, Oberkochen, Germany) using a C-Apochromat 40× (NA = 1.2) objective. Fluorescence in the donor channel (Alexa Fluor546) was excited at 543 nm and recorded in the spectral range 548–628 nm. Directly-excited fluorescence of Alexa Fluor647 was detected in the range of 638–755 nm after excitation at 633 nm. The excitation wavelength of the donor (543 nm) and the emission range of the acceptor (638–755 nm) were used for recording the sensitized emission of the acceptor (FRET channel). Images were analyzed using rFRET, a custom-written program in MATLAB implementing DipImage commands [49]. First, every image was segmented using manually-seeded watershed segmentation. All subsequent calculations were only carried out with membrane pixels constituting the foreground in the resulting mask images. Overspill parameters of the donor were determined using donor-only samples. Overspill of the donor to the FRET channel (parameter S_1) was calculated by fitting a line on the graph of fluorescence in the FRET channel vs. fluorescence in the donor channel using Deming regression. The slope of the line fitted on the graph showing fluorescence in the acceptor channel vs. fluorescence in the donor channel (parameter S_3) was used as the overspill of the donor to the acceptor channel. A similar principle was used to determine acceptor overspill parameters by using cells labeled with the acceptor only. Parameters S_2 and S_4 correspond to the overspill of acceptor fluorescence to the FRET and donor channels, respectively. Furthermore, the α-value corresponding to the ratio of the intensity of an excited acceptor, measured in the FRET channel, to that of an excited donor, measured in the donor channel, was calculated using two microbead samples labeled with equal numbers of donors and acceptors [50]. Once the overspill parameters and the α-value were determined, the FRET efficiency was calculated using the pixel-by-pixel method available in rFRET [51]. Because the laser intensities and detector voltages were adjusted identically in every experiment, the overspill parameters ($S_1 \approx 0.05$, $S_2 \approx 0.03$, $S_3 \approx 9{\cdot}10^{-5}$, $S_4 \approx 0.003$) and the α-value (≈0.6) did not change significantly between experiments.

Measurement of lateral diffusion

CHO cells transfected with GFP-containing constructs of wild-type or mutant ErbB2 were seeded at a density of $2{\cdot}10^4$ cells/well on μ-slide 8-well chambered coverglass (iBIDI) pre-treated with 0.1 mg/mL poly-L-lysine for 15 min and dried for 30 min. Before measurement, the cells were washed with PBS to remove any remaining media, and pre-heated Hank's Balanced Salt Solution was added to the wells. Fluorescence recovery after photobleaching (FRAP) measurements were carried out at 37°C using a C-Apochromat 40× (NA = 1.2) water immersion objective in a Zeiss LSM 880 confocal microscope. The ErbB2-GFP fusion protein was excited at 488 nm, and its fluorescence was detected between 493 and 630 nm. Fluorescence intensity was recorded before and after photobleaching in a predetermined region of interest (ROI) in the cell membrane (bleached ROI). Three images were

taken before bleaching to determine the initial fluorescence intensity, followed by reducing the intensity in the bleached ROI to 30–60% of the initial intensity using the 543 nm laser. Fluorescence recovery was followed until the fluorescence in the bleached ROI stopped increasing (3–4 min). The image series was analyzed in Matlab using a custom-written program, FRAPfit [52]. The stacks were corrected for displacement (registration), and then three ROIs were defined: the bleached ROI, whose coordinates were obtained from the stored stack; the unbleached or total cell ROI generated by watershed segmentation; and the background ROI defined by specifying a cell-free area in the stack. Raw intensity values were triple-normalized, which sets the intensity of the bleached ROI prior to and immediately after the bleaching pulse to 1 and 0, respectively. The following double exponential recovery function was fitted to the triple-normalized curves:

$$R(t) = (1-b)\left[f_1\left(1-e^{-\frac{t}{\tau_1}}\right) + (1-f_1)\left(1-e^{-\frac{t}{\tau_2}}\right)\right] \quad (5)$$

where $R(t)$ is the time-dependent, triple-normalized recovery of fluorescence, b is the immobile fraction, τ_1 and τ_2 are the empirical recovery time constants, and f_1 is the fractional contribution of the first component to the recovery. The amplitude-weighted time constant of the exponential function was calculated and along with the immobile fraction, it was used for characterizing the lateral mobility of the ErbB2 variants. The amplitude-weighted time constant was in the range of 10–40 s, whereas τ_1 and τ_2 ranged from 5 to 25 s, and from 60 to 140 s, respectively. The fast recovery typically accounted for ~50–80% of the total recovery, and both recovery components changed upon EGF treatment. Since no meaningful relationship could be established between the components, the variants and the treatment, and both changed upon EGF stimulation, we report only their amplitude-weighted average in the manuscript.

Two different approaches were used for evaluating and reporting the FRAP data. Individual recovery curves were averaged, and the average curve was fitted to Eq. (5). This approach provides the confidence interval of the fitted parameters, i.e., how precisely the fitted parameters are estimated. A narrow confidence interval means the data constrains that parameter tightly; a wide confidence interval, on the other hand, means the data does not constrain it well. This approach is used in Figures 3BC and 4AB. In the second approach, individual recovery curves were fitted, and the mean and the standard deviation of the fitted parameters are reported. This approach is used in Figure 4EF. While the first approach reveals the reliability of fitting as explained above, the second approach sheds light on potential biological variability. Since biological variability was not significant compared to measurement error, the two approaches gave practically identical results.

Measurement of tyrosine phosphorylation

CHO cells were transiently transfected with the wild-type ErbB2 or one of its mutant variants, or co-transfected with one of the ErbB2 versions and EGFR. To measure baseline ErbB2 phosphorylation in single transfected cells 24 h after transfection, the cells were fixed with 3.7% paraformaldehyde for 30 min at 4°C, followed by permeabilization with 0.1% Triton X-100 for 10 min on ice. For the double-transfected cells, twenty-four hours after transfection, the cells were cultured in serum-starvation medium (0.1% fetal bovine serum) overnight followed by stimulation with 50 nM of EGF for 10 min at 37°C. Afterwards, the cells were fixed and permeabilized as mentioned before. In both cases, after permeabilization, cells were labeled with one of the following primary antibodies in 0.1% BSA + 0.1% Triton X-100 in PBS for 30 min at 4°C: 2.5 μg/mL Ab18 (against ErbB2 phosphorylated at Tyr1248), 1 μg/mL PY99 (pan-phosphotyrosine antibody), 3 μg/mL pEGFR Y1048 or with 2 μg/mL pEGFR Y1173. Staining with primary antibodies was followed by staining with a 4 μg/mL solution of goat anti-mouse Alexa Fluor 647 secondary antibody. After antibody labeling, the cells were fixed with 1% formaldehyde for 20 min at 4°C and visualized by a Nikon N-STORM (Tokyo, Japan) confocal microscope equipped with an Apo 60× water immersion objective. For analysis, images were segmented using manually seeded watershed segmentation based on the GFP channel, generating a mask for cell boundaries. All image analysis was performed in MATLAB (Mathworks, Natick, MA) using custom-written programs implementing DipImage (Delft University of Technology, Delft, The Netherlands) commands. The GFP channel and the PY99-, Ab18-, pEGFR Y1048- or pEGFR Y1173-stained images were extracted to measure tyrosine phosphorylation levels, with the GFP image used for defining regions of interest, and the PY99, Ab18, pEGFR Y1048, or pEGFR Y1173 intensities quantifying phospho-tyrosine levels. Background correction was performed using a region of interest placed in a cell-free area of the image, and background-corrected phosphorylation values were exported for subsequent analysis.

Results

To explore how domain-specific amino acid substitutions alter the membrane behavior of ErbB2, we focused on three clinically relevant ErbB2 missense mutations, R143Q, R678Q and V842I, localized in the extracellular,

juxtamembrane and kinase domains, respectively (Figure 1). These mutations are identified across large pan-cancer cohorts [39,45] or circulating tumor DNA studies [53]. Interestingly, all three mutations have been reported with a frequency of four orders of magnitude higher than expected from the reported human mutation rate in the male germline [42]. This observation highlights their potential relevance as "pre-sensitized" loci that could lead to functional significance upon somatic selection in tumors. We aimed to determine whether the biophysical properties of these mutant receptors are directly linked to their signaling and oncogenic potential, or whether the mutations instead cause more subtle disruptions in receptor oligomerization and diffusion that can only be detected by correlating multiple parameters.

Homo- and heteroclustering of ErbB2 variants measured by Förster resonance energy transfer (FRET)

Since receptor activation begins with alterations in the clustering and lateral diffusion of receptors, we measured the homo- and heteroclusters in CHO cells transiently transfected with different versions of ErbB2 (Figure 2). We compared wild type with two negative controls, a kinase-dead variant (K753M) [54] and a truncated mutant lacking the intercellular domain (ΔIC), two gain-of-function positive controls (+C), V659E [55] and G778D [56], and the three selected ErbB2 variants (R143Q, R678Q and V842I). Although overexpressed ErbB2 is expected to form homodimers or homoclusters [18,57,58], FRET measurements did not provide evidence for strong ErbB2 homoassociation in any of the cell lines transfected with one of the ErbB variants (Figure 2B). While uncertainty in the FRET calibration factor α can potentially lead to an underestimation of the energy transfer efficiency [59], the fact that the ErbB2 variants were identical within experimental error shows that the mutations did not lead to significant changes in their homoassociation tendency. Since CHO cells are practically devoid of endogenous expression of any of the ErbB receptors [60], we co-transfected them with wild-type EGFR and one of the ErbB versions to generate an expression profile more characteristic of the situation *in vivo*. All ErbB2 variants showed heteroassociation with EGFR characterized by a FRET efficiency in the range between 20% and 30% without statistically significant differences (Figure 2C). Stimulation with EGF resulted in a significantly enhanced heterointeraction between EGFR and wild-type ErbB2, and this effect was preserved for the ΔIC variant lacking the whole intracellular domain and the V659E mutant harboring a mutation in the transmembrane domain (Figure 2C). However, neither the kinase-dead (K753M), nor the version with the mutation-activated kinase domain (G778), nor the three selected, cancer-associated ErbB2 variants (R143Q, R678Q, V842I) showed any change in their heteroassociation with EGFR upon EGF treatment. Since the labeling strategy includes labeling control and EGF-treated cells with trastuzumab, we wanted to exclude the possibility that EGF-induced EGFR-ErbB2 heterodimers do not bind the anti-ErbB2 antibody, trastuzumab. Therefore, we compared the fluorescence intensity of trastuzumab in control- and EGF-pretreated cells and found no significant EGF-induced change in the amount of trastuzumab binding to ErbB2 revealing that EGF treatment does not interfere with trastuzumab binding (Suppl. Figure 1A). These experiments also showed that the approximate membrane expression level of ErbB2 was comparable in all samples except for the one transfected with the ΔIC variant, in which the surface expression level of ErbB2 was ~3-fold higher than in the other variants. Additionally, it has been suggested that trastuzumab induces dimerization upon binding [61]. To rule out this possibility, we co-transfected CHO cells with ErbB2 constructs containing YFP or CFP at the N-terminal. The transfected cells were labeled by trastuzumab at 4°C or 37°C and the YFP-CFP heteroassociation was measured. There was no significant difference in ErbB2 homodimerization between the two labeling temperatures indicating that ErbB2 dimerization was not induced by trastuzumab (Suppl. Figure 1B). This result could be due to the largely monovalent binding of bivalent antibodies at concentrations well above their K_d [62]. Next, we analyzed the correlation between the baseline association between ErbB2 and EGFR and the EGF-induced response. If the inactive ErbB2 versions were not considered (ΔIC, K753M), there was a negative correlation characterized by a correlation coefficient of -0.75 between ErbB2/EGFR heteroassociation and the EGF-induced increase thereof. Although the individual ErbB2 versions vary substantially, these results reveal a general tendency whereby variants with higher baseline activation are less likely to respond to EGF stimulation with increased ErbB2–EGFR heterodimerization (Figure 2D).

Lateral mobility of ErbB2 variants measured by fluorescence recovery after photobleaching (FRAP)

We next assessed the lateral diffusion of the ErbB2 variants in living cells to determine how each mutation affects receptor mobility within the membrane (Figure 3). When comparing the lateral mobility of ErbB2 versions expressed as the only member of the ErbB family, the positive controls (V659E, G778D) revealed ~2-fold faster recovery times (Figure 3B) and the V659E variant also showed a ~25% reduced immobile fraction (Figure 3C) than the wild-type, implying higher mobility. The ΔIC variant lacking the whole intracellular domain was even more mobile with a 4-fold lower immobile fraction (Figure 3C) than the

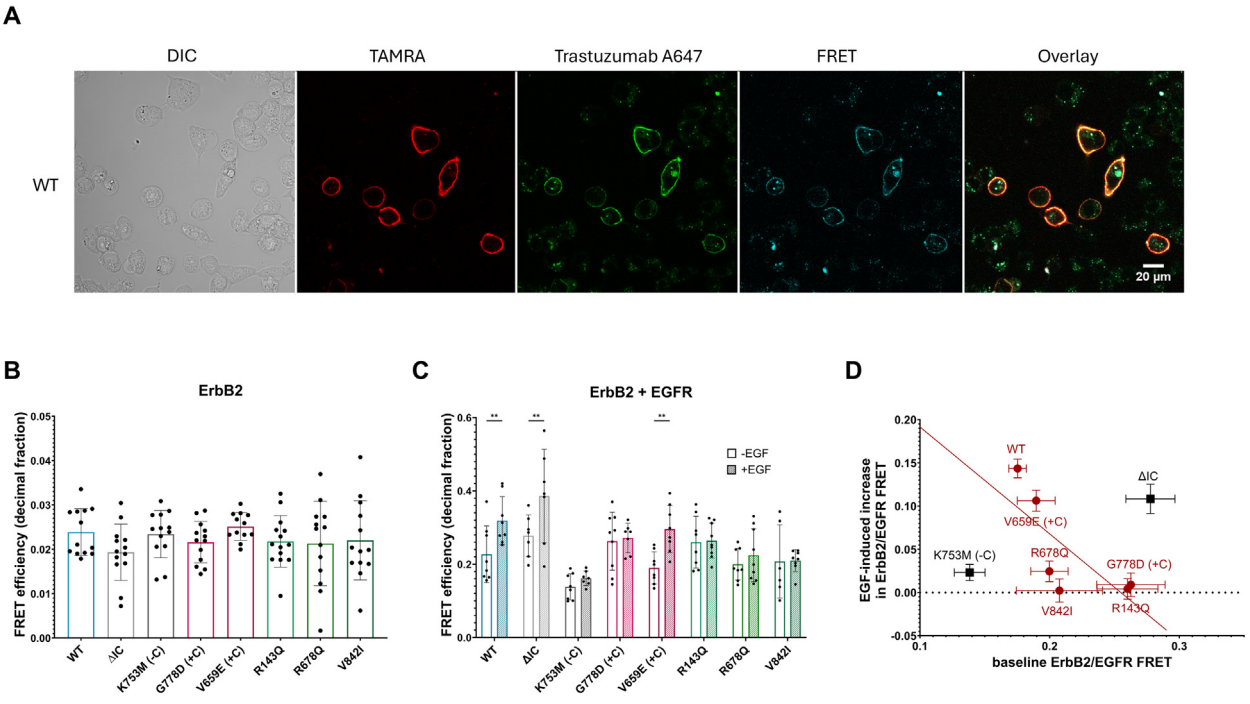

Figure 2. FRET-based analysis of ErbB2 homo- and hetero-association. (**A**) Representative images of cells for FRET measurements. CHO cells were transfected with EGFR and wild-type ErbB2 followed by labeling them with 50 nM TAMRA-EGF for 20 min on ice, followed by 10 min incubation at 37°C for cell stimulation and then labeled with 20 μg/mL AlexaFluor647-trastuzumab for 20 min on ice followed by washing, fixation and confocal microscopic investigation for measuring EGFR-ErbB2 heteroassociation. A differential interference contrast (DIC) image as well as fluorescence images in the donor (TAMRA), acceptor (Trastuzumab A647) and FRET channels were recorded. The overlay of the fluorescence images is shown on the right. (**B**) The homoassociation of wild-type or one of the mutant ErbB2s transfected into CHO cells was measured by confocal microscopic FRET. No significant difference was revealed by one-way analysis of variance. (**C**) CHO cells were transfected with one of the ErbB2 variants and wild-type EGFR followed by overnight serum starvation commencing twenty-four hours after transfection. For measuring quiescent cells, double-labeling with TAMRA-EGF and Alexa Fluor647- trastuzumab was performed on ice preventing the fluorescent EGF from stimulating the cells (empty bars). For measuring EGF-stimulated cells, they were stained with TAMRA-EGF and warmed up to 37°C for 10 min (hatched bars) followed by labeling with Alexa Fluor647-tagged trastuzumab on ice and fixation with 1% PFA. Error bars correspond to the standard deviation. Pairwise comparisons by Sidak multiple comparisons test between untreated and EGF-treated samples were carried out after significant results in two-way ANOVA (**$p < 0.01$). A sample FRET image set is shown in panel A. In panels B and C, the mean ± SD of 10–15 individual measurements from three biological replicates is plotted. An individual measurement represents recording a slide region with ~20 cells, i.e., 3–5 slide regions/biological replicate. (D) The EGF-induced increase in the heteroassociation between ErbB2 and EGFR is plotted against the baseline FRET values for their heteroassociation. The points and the error bars represent the mean and the standard error of the mean, respectively. The red and black symbols correspond to the active and the inactive versions of ErbB2, respectively. The correlation coefficient of the line fitted on the red symbols is −0.75.

WT variant, most likely due to the absence of potential cytoskeletal interactions. The cancer-associated ErbB2 variants, R143Q, R678Q, V842I, exhibited a ~2-fold faster recovery and 10–30% lower immobile fractions compared to the wild-type, resembling the positive controls (Figure 3BC). It can be concluded that the mutationally-activated positive controls and the cancer-associated ErbB2 versions exhibit accelerated diffusion when expressed as the only member of the ErbB family.

We also examined the lateral mobility of the ErbB2 variants in an EGFR-expressing background. The lateral diffusion of wild-type ErbB2 co-expressed with EGFR in the absence of EGF stimulation was 2-fold faster than in cells expressing ErbB2 as the only member of the ErbB family (Figure 4A). Stimulation of these cells with EGF led to retarded diffusion of ErbB2 as revealed by a slower recovery time (Figure 4A) and higher immobile fraction (Figure 4B). The kinase-dead K753M version did not respond to EGF stimulation with regard to its lateral mobility although its baseline mobility did not show any obvious difference from the wild-type before EGF stimulation. All the other versions, including the

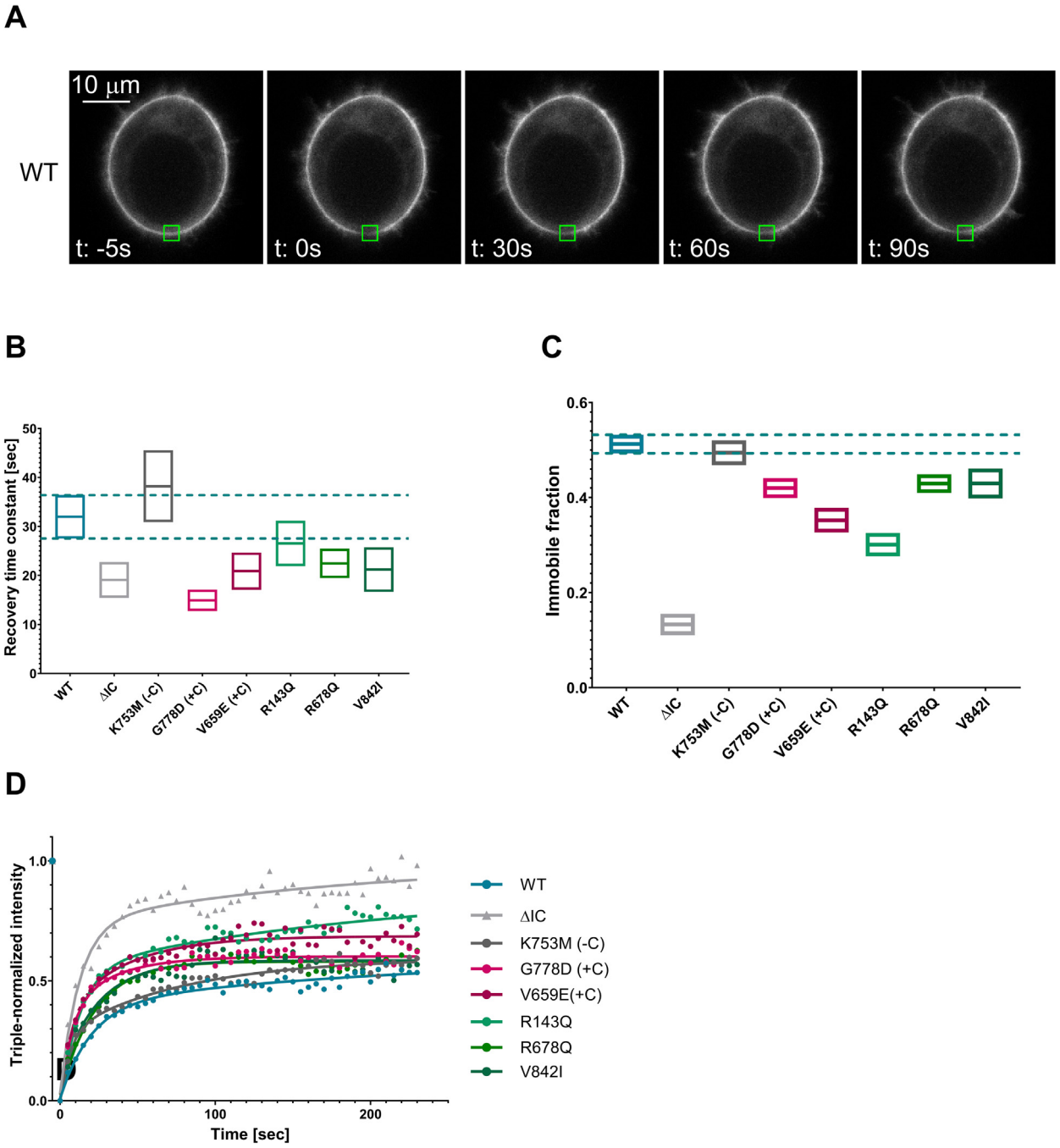

Figure 3. Lateral mobility of ErbB2 variants in the absence of EGFR coexpression. (A) Representative images of cells for FRAP measurements. CHO cells were transfected with EGFR and wild-type ErbB2 and FRAP measurements were performed using the GFP tag present in the wild-type ErbB2 as described in the Methods section. The image sequence shows the pre-bleach image (t: −5 s), the image recorded just after the bleaching pulse (t: 0 s) followed by three images recorded during the recovery period (t: 30 s, 60 s, 90 s). The green rectangle shows the bleached region of interest in which the recovery was monitored. **(B-C)** CHO cells were transfected with one of the ErbB2 variants and FRAP experiments were carried out using the GFP tags of the proteins. Recovery curves were averaged and fitted by a double-exponential function from which the amplitude-weighted recovery time constants (B) and the immobile fractions (C) were determined as described in detail in the Methods section. The fit parameters and their 95% confidence interval are plotted in the graph. (**D**) The FRAP recovery curves recorded for ErbB2-only expressing cells are shown. To obtain the average recovery curves for panels B–C, 15–20 cells (15–20 curves) from five biological replicates were averaged.

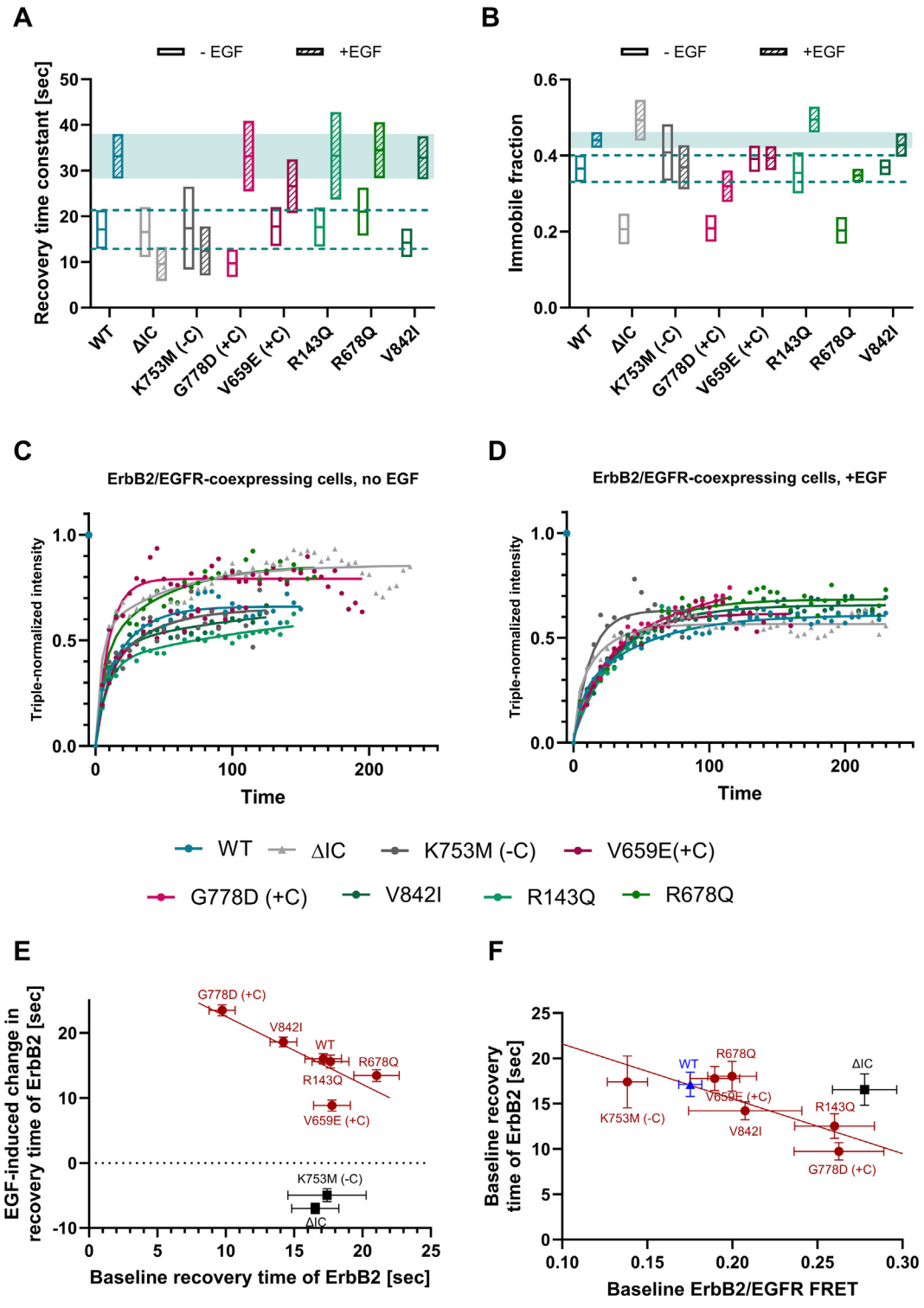
A
- EGF
+EGF
Recovery time constant [sec]
WT
ΔIC
K753M (-C)
G778D (+C)
V659E (+C)
R143Q
R678Q
V842I
B
Immobile fraction
C
ErbB2/EGFR-coexpressing cells, no EGF
Triple-normalized intensity
Time
D
ErbB2/EGFR-coexpressing cells, +EGF
WT
ΔIC
K753M (-C)
V659E(+C)
G778D (+C)
V842I
R143Q
R678Q
E
EGF-induced change in recovery time of ErbB2 [sec]
Baseline recovery time of ErbB2 [sec]
F
Baseline recovery time of ErbB2 [sec]
Baseline ErbB2/EGFR FRET

ΔIC and all the kinase-active variants, responded to EGF by a retarded diffusion without a noticeable correlation between kinase activity and lateral mobility (Figure 4AB). However, when the EGF-induced changes in the lateral diffusion parameters were plotted as a function of their baseline values, an obvious relationship could be spotted (Figure 4EF). Although the negative controls (ΔIC, K753M) stood out from this obvious negative correlation, the rest of the variants established that the more immobile ErbB2 is before EGF stimulation, the less immobilization response it exhibits after EGF challenge (Figure 4E). A weaker, but similar tendency was revealed by the plot of the baseline immobile fraction and its EGF-induced change (data not shown). Although the activated ErbB2 versions (the positive controls and the cancer-associated variants) did not significantly differ from the wild-type in either the heterodimerization or the mobility measurements, plotting their baseline FRAP recovery time constants against ErbB2/EGFR heterodimerization revealed another notable correlation. All the activated ErbB2 variants exhibited higher baseline heterodimerization with EGFR than the wild-type, and they also tended to show higher lateral mobility (Figure 4F). Although the individual differences are not substantial, an obvious correlation emerges when several ErbB2 mutants spanning a wide range of pre-activation states are investigated. This correlation implies that while growth factor-induced dimerization leads to retarded diffusion of ErbB2 (Figure 4AB), its mutational activation is associated with accelerated diffusion both in the absence (Figure 3BC) and in the presence (Figure 4F) of EGFR coexpression.

EGF-induced tyrosine phosphorylation in cells expressing the ErbB2 variants

In order to investigate the biological significance of these ErbB2 mutations at the cellular level, we measured the amount of ErbB2 phosphorylated at Tyr1248 and the general increase in the total cellular amount of phospho-tyrosine. Staining of untransfected and unstimulated cells for tyrosine phosphorylation or secondary staining without prior addition of primary antibodies of transfected cells confirmed the specificity of labeling (Suppl. Figure 2). In CHO cells single-transfected with one of the ErbB2 variants and cultured under normal conditions, i.e., in the presence of serum, ErbB2 tyrosine phosphorylation was 3-fold and 5-fold lower in the ΔIC and K753M mutants, respectively, and 2-fold higher in the constitutively active transmembrane domain mutant (V659E) and the variant harboring a kinase domain with increased activity (G778D) compared to the wild-type (WT) (Figure 5, Suppl. Figure 3). From the studied ErbB2 substitutions, only the kinase domain variant (V842I) showed a higher ErbB2-specific tyrosine phosphorylation (Figure 5A). General tyrosine phosphorylation in cells expressing the ΔIC version was 2-times lower, whereas in cells transfected with the V659E mutant, it was 3-fold higher than in the wild-type (Figure 5B, Suppl. Figure 4). In CHO cells expressing both EGFR and one of the ErbB2 variants, both the baseline tyrosine phosphorylation (in unstimulated, serum-starved

Figure 4. Lateral mobility of ErbB2 variants in the presence of EGFR co-expression. (A–B). For the investigation of ErbB2 variants co-expressed with EGFR, CHO cells were transfected with one of the ErbB2 variants and wild-type EGFR. The cells were serum-starved overnight twenty-four hours after transfection, followed by measuring the lateral mobility of ErbB2 in these unstimulated cells (empty boxes). EGF stimulation was achieved by warming the samples to 37°C on the microscope stage for 10 min allowing the unlabeled EGF, already bound to the cells, to stimulate them followed by measuring the lateral mobility of ErbB2 (hatched boxes). The boxes represent the mean and the 95% confidence interval of the amplitude-weighted recovery time constant (A) and the immobile fraction (B) obtained by fitting the mean recovery curves. **(C–D)** The FRAP recovery curves recorded for ErbB2-EGFR coexpressing cells without (C) and with EGF stimulation (D) are shown. Recovery curves were triple-normalized, setting the pre-bleach and post-bleach intensities to 1 and 0, respectively. 10–20 such individual, triple-normalized curves were averaged, and these mean curves are displayed in the panels C and D. **(E)**. Alternatively, individual curves were also fitted, and the recovery times were averaged to obtain the baseline values and their EGF-induced changes. The EGF-induced change in the mean recovery time constant is plotted against the baseline value before EGF stimulation. The points and the error bars represent the mean and the standard error of the mean, respectively. The red and black symbols correspond to the active and the inactive versions of ErbB2, respectively. The correlation coefficient of the line fitted on the red symbols is −0.91. (**F**) Correlation between baseline FRET values for ErbB2/EGFR heterodimerization and the mobility of ErbB2. The FRAP recovery time constants and FRET values measured for ErbB2/EGFR heterodimerization in the absence of EGF stimulation are plotted against each other. The error bars represent the standard error of the mean. The variant lacking the intracellular domain (ΔIC) and the wild-type are marked by black and blue symbols, respectively. A line was fitted to all the points except the one corresponding to the ΔIC variant ($r = -0.85$).

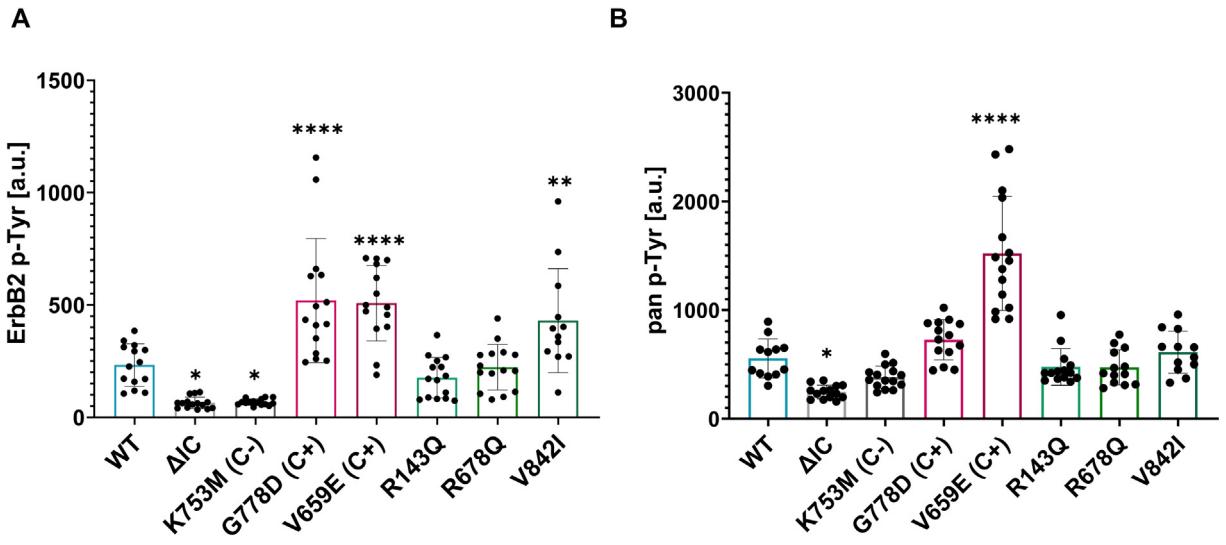

Figure 5. Investigation of tyrosine phosphorylation in ErbB2-only expressing cells. CHO cells transfected with wild-type ErbB2 or one of the mutant variants were stained for ErbB2 phosphorylated at Tyr1248 (A) or with an antibody against any phospho-tyrosine (B) followed by secondary antibody staining and confocal microscopy. Asterisks correspond to significant differences compared to the wild-type determined by Dunnet's test after ANOVA implying significant between-group differences (*$p < 0.05$, ***$p < 0.01$, ****$p < 0.0001$). The error bars in all subpanels in the figure correspond to the standard error of the mean calculated from 15 to 20 images, containing approximately 250 cells, recorded in three independent experiments.

cells) and the EGF-induced response were determined. Regarding baseline general tyrosine phosphorylation, only the constitutively active V659E mutant exhibited a significant, 2-fold increase compared to the WT (Figure 6C, Suppl. Figure 5). We observed a significant, EGF-induced increase in the tyrosine phosphorylation of ErbB2 in all versions except the ΔIC and K753M mutants (Figure 6AB). As far as the EGF-induced increase in general tyrosine phosphorylation is concerned, we observed a similar pattern with the following notable differences (Figure 6C). (i) Although the K753M ErbB2 mutant is kinase-dead, EGF was able to elicit increased pan-tyrosine phosphorylation. (ii) The V659E constitutively active version was so greatly pre-activated in serum-starved cells that no further EGF-induced response could be elicited. (iii) The three variants R143Q, R678Q and V842I responded to EGF-stimulation with the V842I variant having the least response. Moreover, in the co-transfected cells, EGFR phosphorylation was measured at two tyrosine phosphorylation sites, Y1048 (Figure 7A, Suppl. Figure 6) and Y1173 (Figure 7B, Suppl. Figure 7). Out of the three cancer-associated variants, R678Q and V842I showed a ~2-times lower unstimulated pEGFR Y1048 phosphorylation than the WT (Figure 7A) and a similar phosphorylation state at the Y1173 site (Figure 7B). Upon EGF stimulation, none of the cancer-associated variants (R143Q, R678Q, V842I) showed an increase in tyrosine phosphorylation in any of the analyzed tyrosines of EGFR (Figure 7AB).

Although these investigations aimed to reveal potential differences between the activated mutants and the wild-type ErbB2, no obvious correlation could be seen in the tyrosine phosphorylation response itself. Therefore, bivariate analyses were performed and the plot of EGF-induced increase in ErbB2 tyrosine phosphorylation and EGFR-ErbB2 heterodimerization exhibited a remarkable correlation. Although all the ErbB2 versions with a functional kinase domain responded to EGF with a similar change in ErbB2 tyrosine phosphorylation, both positive controls (V659E, G778D) and the three cancer-associated variants achieved this with a lower increase in EGFR-ErbB2 heterodimerization (Suppl. Figure 8A). This correlation was less discernable in the plot of pan-tyrosine phosphorylation and EGFR-ErbB2 heterodimerization (Suppl. Figure 8B). Although for EGFR-ErbB2 heterodimerization and ErbB2 lateral mobility, EGF-induced changes negatively correlated with baseline values (Figures 2D, 3E), no such correlation could be established for the tyrosine phosphorylation response (Suppl. Figure 8C).

In conclusion, neither the tyrosine phosphorylation response, nor the heterointeraction between EGFR and ErbB2 was suitable for discriminating between activated and wild-type ErbB2, their correlated comparison

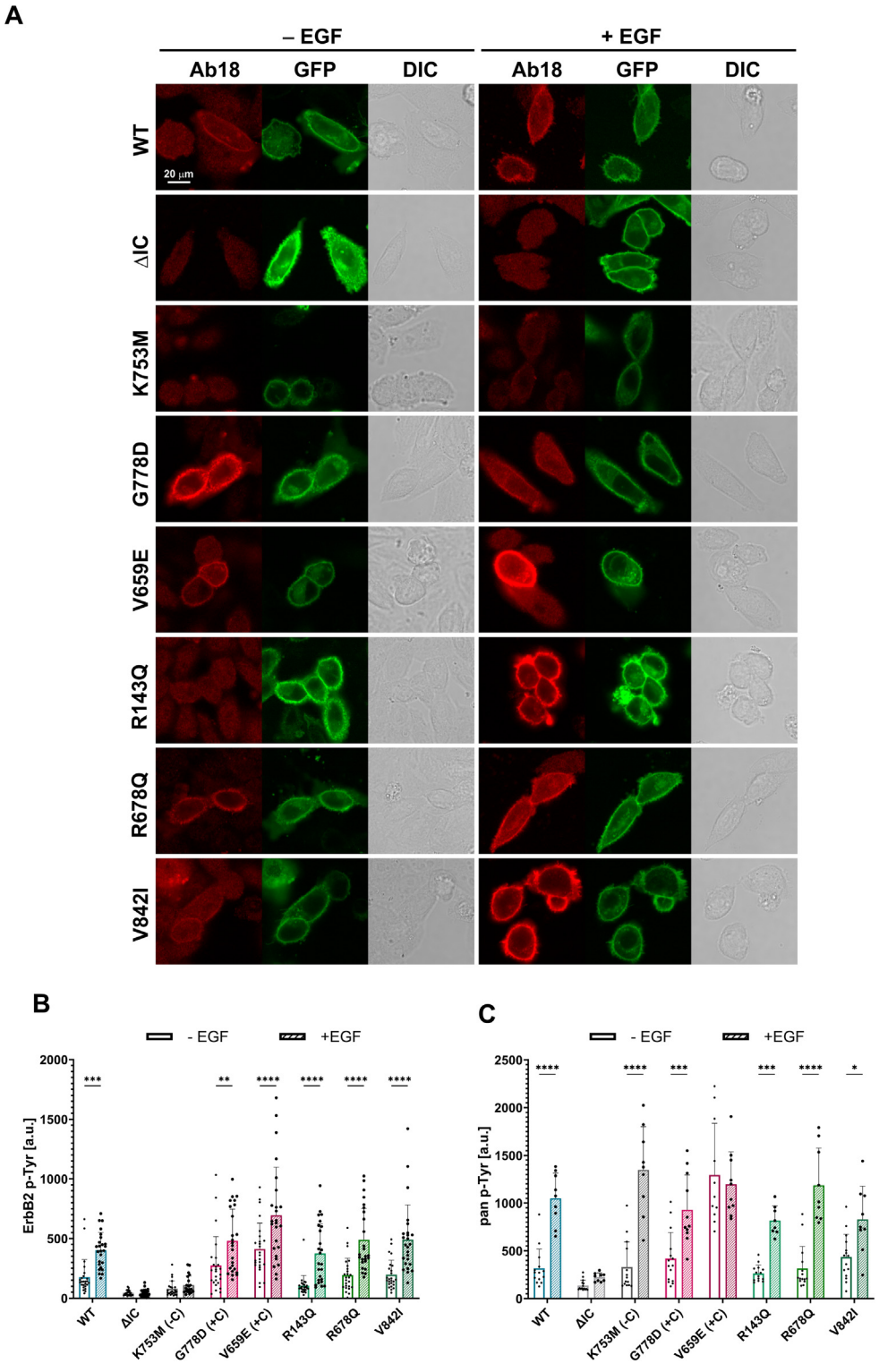
A
– EGF
+ EGF
Ab18
GFP
DIC
WT
ΔIC
K753M
G778D
V659E
R143Q
R678Q
V842I
20 μm
B
- EGF
+EGF
ErbB2 p-Tyr [a.u.]
C
pan p-Tyr [a.u.]

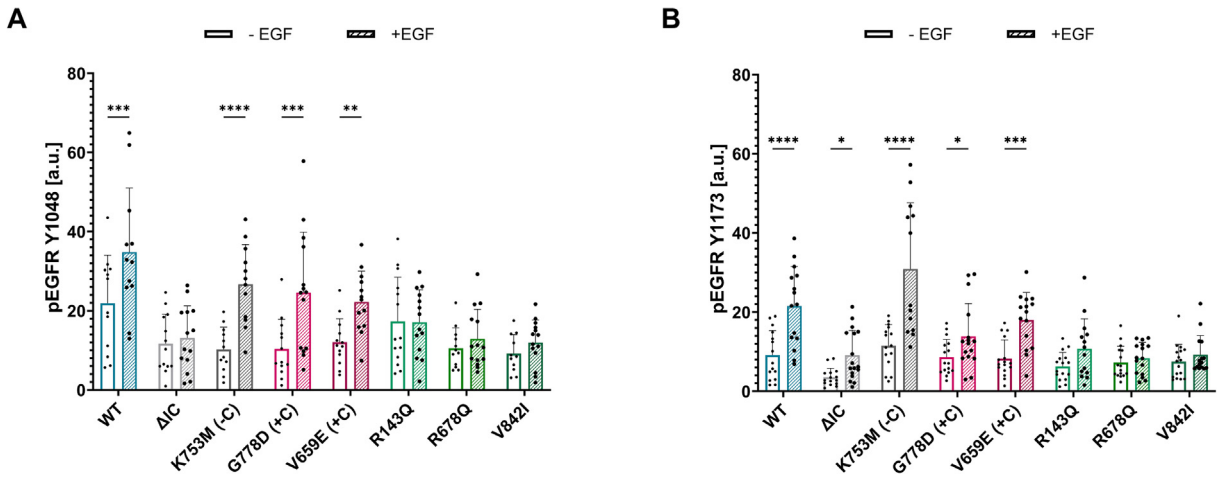

Figure 7. EGFR tyrosine phosphorylation state in cells co-expressing ErbB2 variants. CHO cells double-transfected with EGFR and one of the ErbB2 variants were serum-starved overnight. EGFR phosphorylation at Tyr1048 (A) and Tyr1173 (B) labeled and measured by immunofluorescence was quantified in quiescent cells (empty boxes) and cells stimulated by 50 nM EGF (hatched boxes). The figures show data from approximately 200 cells (∼15 images with 10–15 cells/image from three biological replicates). Pairwise comparisons by Sidak multiple comparisons test between untreated and EGF-treated samples were carried out after significant results in two-way ANOVA (*$p < 0.05$, **$p < 0.01$, ***$p < 0.001$, ****$p < 0.0001$).

revealed that the three ErbB2 cancer-associated variants resembled other activated ErbB2 mutants in that the same tyrosine phosphorylation response required less pronounced growth factor-induced increase in heterodimerization than in the wild-type.

Discussion

The aim of this study was to describe how three clinically relevant ErbB2 variants, R143Q, R678Q and V842I affect the clustering and lateral diffusion of ErbB2 and the ligand-induced reorganization thereof, which will provide insight into the understanding of how single amino acid substitutions distributed across different domains of ErbB2 influence receptor conformation, membrane interactions and dimerization potential. We chose to examine these variants for two main reasons. First, they occur in high frequencies in the human germline [42] and cancer sequencing datasets [45]. Second, they represent strategic structural positions, R143Q in the extracellular domain, R678Q in the juxtamembrane domain, and V842I in the kinase domain. Together with known activating mutants (V659E, G778D) and inactive controls (ΔIC, K753M), these substitutions provide a framework for correlating the biophysical properties of receptors on a wide range of pre-activated states.

When these variants were expressed in the absence of other ErbB proteins, only lateral mobility was predictive of the activation state of the protein with all the activated variants showing

Figure 6. Tyrosine phosphorylation state of ErbB2 variants co-expressed with EGFR. (A) Representative images of the measurement of ErbB2-specific tyrosine phosphorylation are shown. CHO cells cotransfected with EGFR and with one of the ErbB2 variants, displayed on the left, underwent overnight serum starvation twenty-four hours after transfection. Then, the EGF stimulated samples were treated with 50 nM EGF at 37°C for 10 min. Both the stimulated and the control samples were fixed with 3.7% paraformaldehyde at 4°C for 30 min followed by permeabilization with 0.1% Triton X-100 for 10 min. The permeabilized cells were labeled with Ab18 against ErbB2 phosphorylated at Tyr1248 followed by secondary labeling with goat anti-mouse Alexa Fluor 647 secondary antibody. Images recorded in the GFP channel, showing the GFP fluorescence of the ErbB2 constructs, as well as images showing ErbB2 tyrosine phosphorylation along with the transmission images (DIC) are shown in the figure. All images were processed identically to preserve intensity differences. **(B–C)** CHO cells double-transfected with EGFR and one of the ErbB2 variants were serum-starved overnight. ErbB2 phosphorylation at Tyr1248 (B) and pan-tyrosine phosphorylation (C) measured by immunofluorescence as in Figure 5, was quantified in quiescent cells and cells stimulated by 50 nM EGF. The figures show data from approximately 200 cells (∼15 images with 10–15 cells/image from three biological replicates). Pairwise comparisons by Sidak multiple comparisons test between untreated and EGF-treated samples were carried out after significant results in two-way ANOVA (*$p < 0.05$, **$p < 0.01$, ***$p < 0.001$, ****$p < 0.0001$).

accelerated diffusion (Figure 3BC). However, this observation has limited value for human physiology or pathology since ErbB2 is never expressed in the absence of other ErbB receptors. EGF stimulation has been previously shown to induce retarded diffusion of EGFR [15], and our findings also revealed slower diffusion of ErbB2 after EGF stimulation (Figure 4AB). This result contrasted the tendency of mutation-activated ErbB2 variants to exhibit accelerated diffusion (Figure 4F). Although neither lateral diffusion nor ErbB2/EGFR heterointeraction alone appeared to be a reliable marker for activated ErbB2 variants, these mutation-activated versions consistently displayed higher ErbB2/EGFR heterodimerization and faster diffusion in the absence of EGF stimulation, revealing a clear correlation. The opposing effects of growth factor- and mutation-induced activation on the lateral diffusion of ErbB2 suggest that two antagonistic processes are at work. Activation is often associated with increased lateral mobility of receptors [30,63] attributed to increased membrane turnover or cytoskeleton-mediated transport [64]. These effects do not pertain to oligomeric receptors [28] that are hindered in their mobility due to crowding [29] and cytoskeletal anchoring [14]. The former effect may contribute to the increased mobility of activated ErbB mutants in the absence of EGF stimulation (Figure 4F). On the other hand, clustering- and cytoskeleton-dependent effects may cause the retarded lateral mobility of ligand-activated ErbB2 coexpressed with EGFR (Figure 4AB).

Further correlations were revealed by analyzing the EGF-induced responses as a function of the baseline heterodimerization or diffusion properties. The more predimerized with EGFR a certain ErbB2 mutant was, the less EGF-induced heterodimerization it showed with the most pre-heterodimerized variants being practically unresponsive to the growth factor (Figure 2D). Although there was a similar negative correlation for the FRAP recovery time constants (slower baseline diffusion – less EGF-induced retardation of diffusion), all the activated ErbB2 mutants responded to EGF (Figure 4AB). As far as the tyrosine phosphorylation response is concerned, there was no correlation between baseline tyrosine phosphorylation and the EGF response (Suppl. Figure 8C). As a consequence, the same EGF-induced, ErbB2-specific tyrosine phosphorylation response was achieved by less growth factor-dependent increase in heteroassociation in the activated ErbB2 versions (Suppl. Figure 8A).

We propose the following model to account for these observations (Figure 8). Mutation-activated variants of ErbB2 are not all-out activated, but they are predimerized forming ligand-independent, constitutive heterodimers with EGFR. The supramolecular structure of these ligand-independent dimers is not identical to the fully activated dimers since they are not tyrosine phosphorylated and they exhibit slightly accelerated lateral diffusion (Figure 4F). EGF stimulation converts these non-phosphorylated, constitutive dimers to full-fledged, signaling competent dimers characterized by retarded lateral diffusion. As discussed above, mutation-activated ErbB2 displays higher mobility when expressed alone (Figure 3BC) or together with EGFR (Figure 4F), while its ligand-mediated stimulation results in retarded diffusion (Figure 4AB). We suspect that the cytoskeleton may be behind both phenomena. Activation-induced increased membrane turnover and receptor transport may lead to accelerated diffusion via the cytoskeleton [30,63,64] but if oligomerization is extensive and tethering to the cytoskeleton is very stable, retarded diffusion is the consequence [14,15,28,29]. The mechanism of ligand-independent dimerization is not known for all ErbB2 mutants, but the dimerization of the V659E variant is known to be driven by the transmembrane domain [55], and the G778D version with the upregulated kinase activity may be dimerized by the kinase domain since it is known to form dimers reminiscent of the cyclin-CDK complex [65]. This model could account for the contradictory observations made with the R678Q mutant, which behaved as other activated ErbB2 mutants in terms of dimerization [45], but its effect on baseline, ligand-independent signaling was found to be marginal [37]. This contradiction is only apparent and is in fact in perfect agreement with the proposed model, according to which these oncogenic mutations pre-dimerize the receptors without forming full-fledged, signaling-competent dimers.

As far as the kinase-dead, K753M mutant is concerned, it did not respond to EGF by increased EGFR-ErbB2 heterodimerization (Figure 2C), retarded lateral mobility (Figure 4AB) or increased, ErbB2-specific tyrosine phosphorylation (Figure 6B), but the growth factor did increase general tyrosine phosphorylation even in these cells (Figure 6C). This finding is at odds with the sequential, receiver-activator model proposed by Macdonald-Obermann et al [23]. According to this model, EGF-bound EGFR first adopts the receiver role and is activated first, and phosphorylates ErbB2, its heterodimerization partner. Therefore, the heterodimer of a kinase-dead ErbB2 and EGF-bound, wild-type EGFR should be kinase-active since the wild-type, EGF-bound EGFR should be activated by the kinase-dead ErbB2 allowing ErbB2 to be transphosphorylated. In their experiments, Tyr-1221 of the kinase-dead ErbB2 was phosphorylated, whereas we could not detect phosphorylation of Tyr-1248 of ErbB2 under the same circumstances. Additionally, no EGF-induced EGFR phosphorylation at tyrosines Y1048 (Figure 7A) and Y1173 (Figure 7B) was detected in cells coexpressing EGFR with one of the cancer-associated ErbB2 mutants. These results support the idea that, in

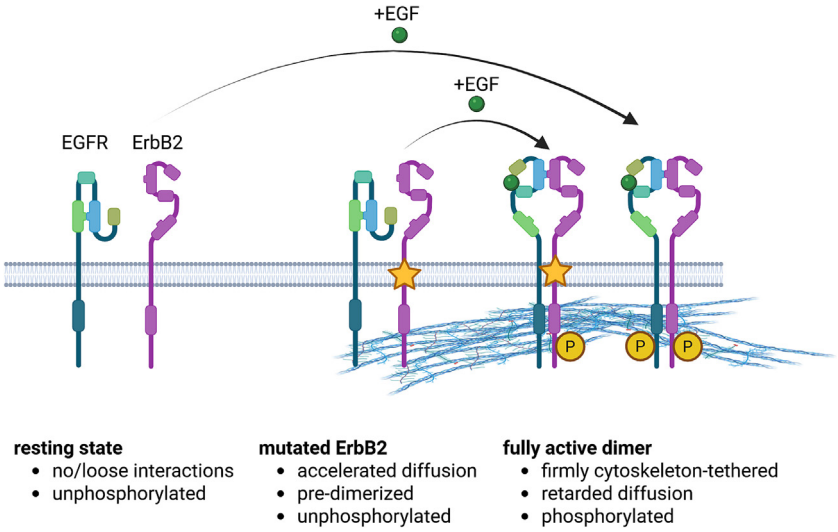

Figure 8. Model for heterodimerization of EGFR with wild-type and mutation-activated ErbB2. In the absence of growth factor stimulation, wild-type ErbB2 and EGFR are mostly monomeric, although the non-zero FRET efficiency characterizing constitutive EGFR/ErbB2 heterodimerization suggests that some kind of loose association may take place (not displayed in the figure). Activation by mutation induces ligand-independent dimerization in the absence of appreciable amount of tyrosine phosphorylation. Mutation-activated ErbB2 is labeled by a star symbol in the transmembrane domain although the activating mutation is not necessarily present in this part of the protein. These constitutive dimers display slightly elevated lateral diffusion whose reason is unknown, but may be related to cytoskeleton-mediated increased membrane turnover or receptor transport. Growth factor-dependent activation of either kind of heterodimer results in the formation of fully active, phosphorylated dimers firmly anchored to the cytoskeleton. The conformation and arrangement of monomers in the pre-dimerized, mutation-activated heterodimers and in the ligand-dependent dimers are displayed only schematically since extensive interactions are known to take place between the extracellular, transmembrane and kinase domains in ligand-activated dimers, and these interactions are most likely different in the non-fully functional dimers formed by mutation-activated ErbB2 (figure created in BioRender.com).

addition to catalytic competence, the precise structural alignment along the receptor domains is necessary for EGFR-ErbB2 heterodimer activation. Such mutations may destabilize the active, asymmetric dimer or alter receptor trafficking and clustering, thereby impeding receptor transactivation [66]. These results suggest that either the sequential activation model proposed by Macdonald-Obermann is context-dependent, or EGFR cannot phosphorylate Tyr-1248 of ErbB2. Further experiments will be required to resolve this contradiction.

In summary, our findings show that single amino acid substitutions may influence receptor organization, membrane dynamics, and ligand responsiveness. Our results highlight that catalytic activity and conformational integrity are both required for a successful EGFR-ErbB2 heterodimer activation. The absence of EGFR and ErbB2 phosphorylation in kinase-impaired mutants or the altered phosphorylation in the studied cancer-associated mutants indicates that precise receptor alignment is essential for maintaining an active dimer configuration. Altogether, these results and the model presented in the current manuscript show that the relationship between the biophysical and signaling properties of receptors is complex that can only be revealed by a correlated multiparameter analysis.

CRediT authorship contribution statement

Tayde Gabriela Serrano Cano: Writing – original draft, Methodology, Investigation, Formal analysis. **Atena Yasari:** Methodology, Investigation. **Ingrid Hartl:** Investigation, Funding acquisition. **Irene Tiemann-Boege:** Writing – review & editing, Funding acquisition, Conceptualization. **Peter Nagy:** Writing – review & editing, Supervision, Funding acquisition, Conceptualization.

DATA AVAILABILITY

Data will be made available on request.

DECLARATION OF COMPETING INTEREST

The authors declare the following financial interests/personal relationships which may be considered as potential competing interests: Peter Nagy reports financial support was provided by

National Research, Development and Innovation Office. Ingrid Hartl reports financial support was provided by Austrian Science Fund. Irene Tiemann-Boege reports financial support was provided by Austrian Science Fund. Irene Tiemann-Boege reports financial support was provided by European Regional Development Fund. Peter Nagy reports financial support was provided by University of Debrecen. If there are other authors, they declare that they have no known competing financial interests or personal relationships that could have appeared to influence the work reported in this paper.

Acknowledgments

This work was supported by the National Research, Development and Innovation Office, Hungary (ANN133421, K138075); the Austrian Science Fund (FWFW1250, P30867000); the European Regional Development Fund (REGGEN ATCZ207), and by the University of Debrecen.

Appendix A. Supplementary material

Supplementary material to this article can be found online at https://doi.org/10.1016/j.jmb.2026.169770.

Received 18 November 2025;
Accepted 24 March 2026;
Available online 28 March 2026

Keywords:
ErbB2;
dimerization;
oligomerization;
lateral diffusion;
tyrosine phosphorylation

References

[1]. Bublil, E.M., Yarden, Y., (2007). The EGF receptor family: spearheading a merger of signaling and therapeutics. *Curr. Opin. Cell Biol.* **19**, 124–134. https://doi.org/10.1016/j.ceb.2007.02.008.

[2]. Stein, R.A., Staros, J.V., (2006). Insights into the evolution of the ErbB receptor family and their ligands from sequence analysis. *BMC Evol. Biol.* **6**, 79. https://doi.org/10.1186/1471-2148-6-79.

[3]. Falls, D., (2003). Neuregulins: functions, forms, and signaling strategies. *Exp. Cell Res.* **284**, 14–30. https://doi.org/10.1016/S0014-4827(02)00102-7.

[4]. Klapper, L.N., Glathe, S., Vaisman, N., Hynes, N.E., Andrews, G.C., Sela, M., et al., (1999). The ErbB-2/HER2 oncoprotein of human carcinomas may function solely as a shared coreceptor for multiple stroma-derived growth factors. *PNAS* **96**, 4995–5000. https://doi.org/10.1073/pnas.96.9.4995.

[5]. Citri, A., Yarden, Y., (2006). EGF–ERBB signalling: towards the systems level. *Nature Rev. Mol. Cell Biol.* **7**, 505–516. https://doi.org/10.1038/nrm1962.

[6]. Kovacs, T., Zakany, F., Nagy, P., (2022). It takes more than two to tango: complex, hierarchal, and membrane-modulated interactions in the regulation of receptor tyrosine kinases. *Cancers* **14**, 944. https://doi.org/10.3390/cancers14040944.

[7]. Dawson, J.P., Bu, Z., Lemmon, M.A., (2007). Ligand-induced structural transitions in ErbB receptor extracellular domains. *Structure* **15**, 942–954. https://doi.org/10.1016/j.str.2007.06.013.

[8]. Alvarado, D., Klein, D.E., Lemmon, M.A., (2009). ErbB2 resembles an autoinhibited invertebrate epidermal growth factor receptor. *Nature* **461**, 287–291. https://doi.org/10.1038/nature08297.

[9]. Garrett, T.P.J., McKern, N.M., Lou, M., Elleman, T.C., Adams, T.E., Lovrecz, G.O., et al., (2003). The crystal structure of a truncated ErbB2 ectodomain reveals an active conformation, poised to interact with other ErbB receptors. *Mol. Cell* **11**, 495–505. https://doi.org/10.1016/S1097-2765(03)00048-0.

[10]. Ogiso, H., Ishitani, R., Nureki, O., Fukai, S., Yamanaka, M., Kim, J.-H., et al., (2002). Crystal structure of the complex of human epidermal growth factor and receptor extracellular domains. *Cell* **110**, 775–787. https://doi.org/10.1016/S0092-8674(02)00963-7.

[11]. Freed, D.M., Bessman, N.J., Kiyatkin, A., Salazar-Cavazos, E., Byrne, P.O., Moore, J.O., et al., (2017). EGFR ligands differentially stabilize receptor dimers to specify signaling kinetics. *Cell* **171**, 683–695.e18. https://doi.org/10.1016/j.cell.2017.09.017.

[12]. Bai, X., Sun, P., Wang, X., Long, C., Liao, S., Dang, S., et al., (2023). Structure and dynamics of the EGFR/HER2 heterodimer. *Cell Discov.* **9**, 18. https://doi.org/10.1038/s41421-023-00523-5.

[13]. Diwanji, D., Trenker, R., Thaker, T.M., Wang, F., Agard, D.A., Verba, K.A., et al., (2021). Structures of the HER2–HER3–NRG1β complex reveal a dynamic dimer interface. *Nature* **600**, 339–343. https://doi.org/10.1038/s41586-021-04084-z.

[14]. Low-Nam, S.T., Lidke, K.A., Cutler, P.J., Roovers, R.C., Van Bergen En Henegouwen, P.M.P., Wilson, B.S., et al., (2011). ErbB1 dimerization is promoted by domain co-confinement and stabilized by ligand binding. *Nature Struct. Mol. Biol.* **18**, 1244–1249. https://doi.org/10.1038/nsmb.2135.

[15]. Vámosi, G., Friedländer-Brock, E., Ibrahim, S.M., Brock, R., Szöllősi, J., Vereb, G., (2019). EGF receptor stalls upon activation as evidenced by complementary fluorescence correlation spectroscopy and fluorescence recovery after photobleaching measurements. *IJMS* **20**, 3370. https://doi.org/10.3390/ijms20133370.

[16]. Lenferink, A.E.G., (1998). Differential endocytic routing of homo- and hetero-dimeric ErbB tyrosine kinases confers signaling superiority to receptor heterodimers. *EMBO J.* **17**, 3385–3397. https://doi.org/10.1093/emboj/17.12.3385.

[17]. Olayioye, M.A., (2000). NEW EMBO MEMBERS' REVIEW: the ErbB signaling network: receptor heterodimerization in development and cancer. *EMBO J.*

19, 3159–3167. https://doi.org/10.1093/emboj/19.13.3159.

[18]. Szabó, Á., Horváth, G., Szöllősi, J., Nagy, P., (2008). Quantitative characterization of the large-scale association of ErbB1 and ErbB2 by flow cytometric homo-FRET measurements. *Biophys. J.* **95**, 2086–2096. https://doi.org/10.1529/biophysj.108.133371.

[19]. Zanetti-Domingues, L.C., Korovesis, D., Needham, S.R., Tynan, C.J., Sagawa, S., Roberts, S.K., et al., (2018). The architecture of EGFR's basal complexes reveals autoinhibition mechanisms in dimers and oligomers. *Nature Commun.* **9**, 4325. https://doi.org/10.1038/s41467-018-06632-0.

[20]. Moradi, Y., Lee, J.S.H., Armani, A.M., (2024). Detecting disruption of HER2 membrane protein organization in cell membranes with nanoscale precision. *ACS Sens.* **9**, 52–61. https://doi.org/10.1021/acssensors.3c01437.

[21]. Zhang, X., Gureasko, J., Shen, K., Cole, P.A., Kuriyan, J., (2006). An allosteric mechanism for activation of the kinase domain of epidermal growth factor receptor. *Cell* **125**, 1137–1149. https://doi.org/10.1016/j.cell.2006.05.013.

[22]. Littlefield, P., Liu, L., Mysore, V., Shan, Y., Shaw, D.E., Jura, N., (2014). Structural analysis of the EGFR/HER3 heterodimer reveals the molecular basis for activating HER3 mutations. *Sci. Signal.* **7** https://doi.org/10.1126/scisignal.2005786.

[23]. Macdonald-Obermann, J.L., Piwnica-Worms, D., Pike, L. J., (2012). Mechanics of EGF Receptor/ErbB2 kinase activation revealed by luciferase fragment complementation imaging. *PNAS* **109**, 137–142. https://doi.org/10.1073/pnas.1111316109.

[24]. Ward, M.D., Leahy, D.J., (2015). Kinase activator-receiver preference in ErbB heterodimers is determined by intracellular regions and is not coupled to extracellular asymmetry. *J. Biol. Chem.* **290**, 1570–1579. https://doi.org/10.1074/jbc.M114.612085.

[25]. Coskun, Ü., Grzybek, M., Drechsel, D., Simons, K., (2011). Regulation of human EGF receptor by lipids. *PNAS* **108**, 9044–9048. https://doi.org/10.1073/pnas.1105666108.

[26]. Schmick, M., Bastiaens, P.I.H., (2014). The interdependence of membrane shape and cellular signal processing. *Cell* **156**, 1132–1138. https://doi.org/10.1016/j.cell.2014.02.007.

[27]. Kovács, T., Batta, G., Hajdu, T., Szabó, Á., Váradi, T., Zákány, F., et al., (2016). The dipole potential modifies the clustering and ligand binding affinity of ErbB proteins and their signaling efficiency. *Sci. Rep.* **6**, 35850. https://doi.org/10.1038/srep35850.

[28]. Bag, N., Huang, S., Wohland, T., (2015). Plasma membrane organization of epidermal growth factor receptor in resting and ligand-bound states. *Biophys. J.* **109**, 1925–1936. https://doi.org/10.1016/j.bpj.2015.09.007.

[29]. Ramadurai, S., Holt, A., Krasnikov, V., Van Den Bogaart, G., Killian, J.A., Poolman, B., (2009). Lateral diffusion of membrane proteins. *J. Am. Chem. Soc.* **131**, 12650–12656. https://doi.org/10.1021/ja902853g.

[30]. Sergé, A., Fourgeaud, L., Hémar, A., Choquet, D., (2002). Receptor activation and homer differentially control the lateral mobility of metabotropic glutamate receptor 5 in the neuronal membrane. *J. Neurosci.* **22**, 3910–3920. https://doi.org/10.1523/JNEUROSCI.22-10-03910.2002.

[31]. Di Fiore, P.P., Pierce, J.H., Kraus, M.H., Segatto, O., King, C.R., Aaronson, S.A., (1987). *erb* B-2 is a potent oncogene when overexpressed in NIH/3T3 cells. *Science* **237**, 178–182. https://doi.org/10.1126/science.2885917.

[32]. Zaczek, A., Wełnicka-Jaśkiewicz, M., Bielawski, K.P., Jaśkiewicz, J., Badzio, A., Olszewski, W., et al., (2008). Gene copy numbers of HER family in breast cancer. *J. Cancer Res. Clin. Oncol.* **134**, 271–279. https://doi.org/10.1007/s00432-007-0284-z.

[33]. Herter-Sprie, G.S., Greulich, H., Wong, K.-K., (2013). Activating mutations in ERBB2 and their impact on diagnostics and treatment. *Front. Oncol.* **3** https://doi.org/10.3389/fonc.2013.00086.

[34]. Petrosino, M., Novak, L., Pasquo, A., Chiaraluce, R., Turina, P., Capriotti, E., et al., (2021). Analysis and interpretation of the impact of missense variants in cancer. *IJMS* **22**, 5416. https://doi.org/10.3390/ijms22115416.

[35]. Subramanian, J., Katta, A., Masood, A., Vudem, D.R., Kancha, R.K., (2019). Emergence of ERBB2 mutation as a biomarker and an actionable target in solid cancers. *Oncologist* **24**, e1303–e1314. https://doi.org/10.1634/theoncologist.2018-0845.

[36]. Stefl, S., Nishi, H., Petukh, M., Panchenko, A.R., Alexov, E., (2013). Molecular mechanisms of disease-causing missense mutations. *J. Mol. Biol.* **425**, 3919–3936. https://doi.org/10.1016/j.jmb.2013.07.014.

[37]. Bose, R., Kavuri, S.M., Searleman, A.C., Shen, W., Shen, D., Koboldt, D.C., et al., (2013). Activating HER2 mutations in HER2 gene amplification negative breast cancer. *Cancer Discov.* **3**, 224–237. https://doi.org/10.1158/2159-8290.CD-12-0349.

[38]. Pon, J.R., Marra, M.A., (2015). Driver and passenger mutations in cancer. *Annu. Rev. Pathol.: Mech. Dis.* **10**, 25–50. https://doi.org/10.1146/annurev-pathol-012414-040312.

[39]. Wang, H., Miao, J., Wen, Y., Xia, X., Chen, Y., Huang, M., et al., (2022). Molecular landscape of ERBB2 alterations in 14,956 solid tumors. *Pathol. Oncol. Res.* **28**, 1610360. https://doi.org/10.3389/pore.2022.1610360.

[40]. Giacoletto, C.J., Valente, L.J., Brown, L., Patterson, S., Gokhale, R., Mockus, S.M., et al., (2025). New gain-of-function mutations prioritize mechanisms of HER2 activation. *medRxiv*2025.03.03.25323043. https://doi.org/10.1101/2025.03.03.25323043.

[41]. Brodeur, M.N., Selenica, P., Ma, W., Moufarrij, S., Dagher, C., Basili, T., et al., (2024). ERBB2 mutations define a subgroup of endometrial carcinomas associated with high tumor mutational burden and the microsatellite instability-high (MSI-H) molecular subtype. *Mol. Oncol.* **18**, 2356–2368. https://doi.org/10.1002/1878-0261.13698.

[42]. Yasari, A., Heinzl, M., Mair, T., Karimian, T., Moukbel, S. A., Hartl, I., et al., (2024). Mutations in ErbB2 accumulating in the male germline measured by error-corrected sequencing. *bioRxiv*. https://doi.org/10.1101/2024.08.14.607923.

[43]. Yi, Z., Rong, G., Guan, Y., Li, J., Chang, L., Li, H., et al., (2020). Molecular landscape and efficacy of HER2-targeted therapy in patients with HER2-mutated metastatic breast cancer. *npj Breast Cancer* **6**, 59. https://doi.org/10.1038/s41523-020-00201-9.

[44]. Kavuri, S.M., Jain, N., Galimi, F., Cottino, F., Leto, S.M., Migliardi, G., et al., (2015). HER2 activating mutations are

targets for colorectal cancer treatment. *Cancer Discov.* **5**, 832–841. https://doi.org/10.1158/2159-8290.CD-14-1211.

[45]. Pahuja, K.B., Nguyen, T.T., Jaiswal, B.S., Prabhash, K., Thaker, T.M., Senger, K., et al., (2018). Actionable activating oncogenic ERBB2/HER2 transmembrane and juxtamembrane domain mutations. *Cancer Cell* **34**, 792–806.e5. https://doi.org/10.1016/j.ccell.2018.09.010.

[46]. De Martino, M., Zhuang, D., Klatte, T., Rieken, M., Rouprêt, M., Xylinas, E., et al., (2014). Impact of *ERBB2* mutations on in vitro sensitivity of bladder cancer to lapatinib. *Cancer Biol. Ther.* **15**, 1239–1247. https://doi.org/10.4161/cbt.29687.

[47]. Liang, Y., Chiu, P.-K.-F., Zhu, Y., Wong, C.-Y.-P., Xiong, Q., Wang, L., et al., (2022). Whole-exome sequencing reveals a comprehensive germline mutation landscape and identifies twelve novel predisposition genes in Chinese prostate cancer patients. *PLoS Genet.* **18**, e1010373. https://doi.org/10.1371/journal.pgen.1010373.

[48]. Brock, R., Hamelers, I.H.L., Jovin, T.M., (1999). Comparison of fixation protocols for adherent cultured cells applied to a GFP fusion protein of the epidermal growth factor receptor. *Cytometry* **35**, 353–362. https://doi.org/10.1002/(SICI)1097-0320(19990401)35:4%253C353::AID-CYTO8%253E3.0.CO;2-M.

[49]. Nagy, P., Szabó, Á., Váradi, T., Kovács, T., Batta, G., Szöllősi, J., (2016). rFRET: a comprehensive, Matlab-based program for analyzing intensity-based ratiometric microscopic FRET experiments. *Cytometry Pt A* **89**, 376–384. https://doi.org/10.1002/cyto.a.22828.

[50]. Batta, Á., Hajdu, T., Nagy, P., (2023). Improved estimation of the ratio of detection efficiencies of excited acceptors and donors for FRET measurements. *Cytometry Pt A* **103**, 563–574. https://doi.org/10.1002/cyto.a.24728.

[51]. Szabó, Á., Szöllősi, J., Nagy, P., (2022). Principles of resonance energy transfer. *Current Protocols* **2**, e625.

[52]. Batta, G., Hajdu, T., Nagy, P., (2021). Characterization of the effect of sphingolipid accumulation on membrane compactness, dipole potential, and mobility of membrane components. In: Bieberich, E. (Ed.), *Lipid Rafts*, **vol. 2187** Springer US, New York, NY, pp. 283–301. https://doi.org/10.1007/978-1-0716-0814-2_16.

[53]. Loree, J.M., Bailey, A.M., Johnson, A.M., Yu, Y., Wu, W., Bristow, C.A., et al., (2018). Molecular landscape of *ERBB2/ERBB3* mutated colorectal cancer. *JNCI: J Natl Cancer Instit* **110**, 1409–1417. https://doi.org/10.1093/jnci/djy067.

[54]. Klos, K.S., Wyszomierski, S.L., Sun, M., Tan, M., Zhou, X., Li, P., et al., (2006). ErbB2 increases vascular endothelial growth factor protein synthesis via activation of mammalian target of Rapamycin/p70S6K leading to increased angiogenesis and spontaneous metastasis of human breast cancer cells. *Cancer Res.* **66**, 2028–2037. https://doi.org/10.1158/0008-5472.CAN-04-4559.

[55]. Fleishman, S.J., Schlessinger, J., Ben-Tal, N., (2002). A putative molecular-activation switch in the transmembrane domain of erbB2. *PNAS* **99**, 15937–15940. https://doi.org/10.1073/pnas.252640799.

[56]. Fan, Y.-X., Wong, L., Ding, J., Spiridonov, N.A., Johnson, R.C., Johnson, G.R., (2008). Mutational activation of ErbB2 reveals a new protein kinase autoinhibition mechanism. *J. Biol. Chem.* **283**, 1588–1596. https://doi.org/10.1074/jbc.M708116200.

[57]. Nagy, P., Bene, L., Balázs, M., Hyun, W.C., Lockett, S.J., Chiang, N.Y., et al., (1998). EGF-induced redistribution of erbB2 on breast tumor cells: flow and image cytometric energy transfer measurements. *Cytometry* **32**, 120–131. https://doi.org/10.1002/(sici)1097-0320(19980601)32:2%253C120::aid-cyto7%253E3.0.co;2-p.

[58]. Nagy, P., Claus, J., Jovin, T.M., Arndt-Jovin, D.J., (2010). Distribution of resting and ligand-bound ErbB1 and ErbB2 receptor tyrosine kinases in living cells using number and brightness analysis. *PNAS* **107**, 16524–16529. https://doi.org/10.1073/pnas.1002642107.

[59]. Agam, G., Gebhardt, C., Popara, M., Mächtel, R., Folz, J., Ambrose, B., et al., (2023). Reliability and accuracy of single-molecule FRET studies for characterization of structural dynamics and distances in proteins. *Nature Methods* **20**, 523–535. https://doi.org/10.1038/s41592-023-01807-0.

[60]. Tzahar, E., Waterman, H., Chen, X., Levkowitz, G., Karunagaran, D., Lavi, S., et al., (1996). A hierarchical network of interreceptor interactions determines signal transduction by neu differentiation factor/neuregulin and epidermal growth factor. *Mol. Cell. Biol.* **16**, 5276–5287. https://doi.org/10.1128/MCB.16.10.5276.

[61]. Maadi, H., Nami, B., Tong, J., Li, G., Wang, Z., (2018). The effects of trastuzumab on HER2-mediated cell signaling in CHO cells expressing human HER2. *BMC Cancer* **18**, 238. https://doi.org/10.1186/s12885-018-4143-x.

[62]. Van Steeg, T.J., Bergmann, K.R., Dimasi, N., Sachsenmeier, K.F., Agoram, B., (2016). The application of mathematical modelling to the design of bispecific monoclonal antibodies. *MAbs* **8**, 585–592. https://doi.org/10.1080/19420862.2016.1141160.

[63]. Alenghat, F.J., Golan, D.E., (2013). Membrane protein dynamics and functional implications in mammalian cells. *Curr. Top. Membr.* **72**, 89–120. https://doi.org/10.1016/B978-0-12-417027-8.00003-9.

[64]. Jacobson, K., Liu, P., Lagerholm, B.C., (2019). The lateral organization and mobility of plasma membrane components. *Cell* **177**, 806–819. https://doi.org/10.1016/j.cell.2019.04.018.

[65]. Jura, N., Zhang, X., Endres, N.F., Seeliger, M.A., Schindler, T., Kuriyan, J., (2011). Catalytic control in the EGF receptor and its connection to general kinase regulatory mechanisms. *Mol. Cell* **42**, 9–22. https://doi.org/10.1016/j.molcel.2011.03.004.

[66]. Hartman, Z., Zhao, H., Agazie, Y.M., (2013). HER2 stabilizes EGFR and itself by altering autophosphorylation patterns in a manner that overcomes regulatory mechanisms and promotes proliferative and transformation signaling. *Oncogene* **32**, 4169–4180. https://doi.org/10.1038/onc.2012.418.

SUPPLEMENTARY MATERIAL

Biophysical characterization of recurrent ErbB2 missense mutations reveals alterations in receptor organization and membrane dynamics

Tayde Gabriela Serrano Cano[1], Atena Yasari[2], Ingrid Hartl[2], Irene Tiemann-Boege[2], Peter Nagy[1]

[1]Department of Biophysics and Cell Biology, Faculty of Medicine, University of Debrecen, Debrecen, Hungary

[2]Institute of Biophysics, Johannes Kepler University, Linz, Austria

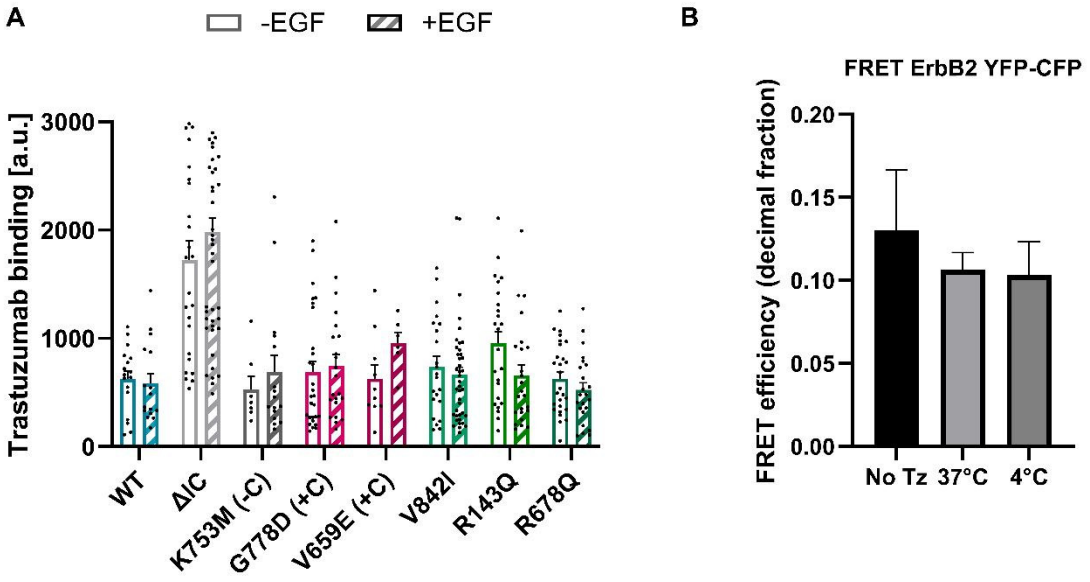

Supplementary Figure 1. Lack of interference of trastuzumab with the measurements. (A) CHO cells double-transfected with EGFR and one of the ErbB2 variants were stimulated with 50 nM unlabeled EGF or left untreated. Both kinds of samples were subsequently stained with AlexaFluor647-trastuzumab, and the fluorescence intensity of trastuzumab was evaluated in the cell membrane. The bars show the mean (±SD) of fluorescence intensity of trastuzumab in the control and the EGF-pretreated samples. None of the pairwise comparisons revealed any significant difference in the binding of trastuzumab between the control and the EGF-treated samples. **(B)** CHO cells were transfected with plasmids pcDNA3-ErbB2-YFP and pcDNA3-ErbB2-CFP, were labeled at 4°C and 37°C for 30 min, followed by washing, fixation and confocal microscopic investigation for measuring ErbB2-YFP and ErbB2-CFP heteroassociation. No significant difference was revealed by one-way analysis of variance indicating the lack of effect of trastuzumab on ErbB2 homoassociation.

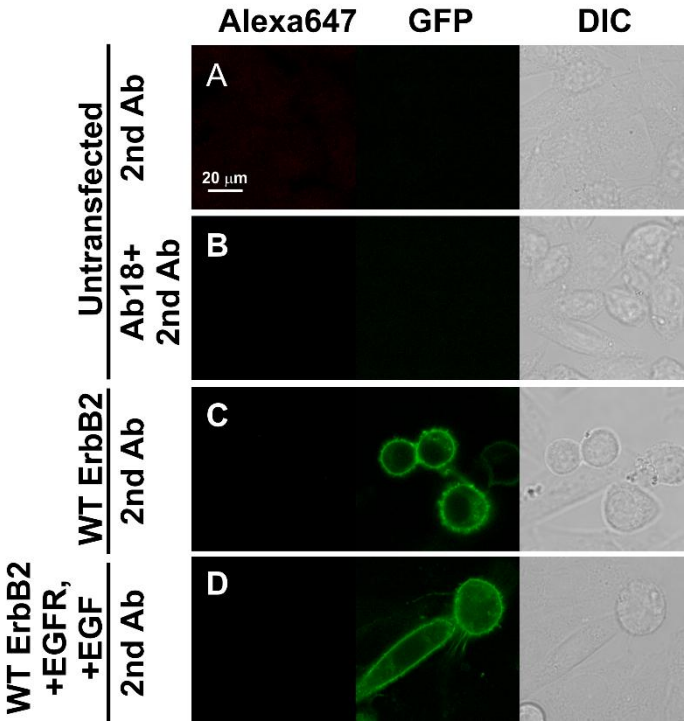

Supplementary Figure 2. Control samples showing specificity of antibody labeling. Untransfected CHO cells were fixed with 3.7% paraformaldehyde at 4°C for 30 minutes followed by permeabilization with 0.1% Triton X-100 for 10 minutes and staining with anti-mouse Alexa Fluor 647 secondary antibody (A) or with Ab18 against ErbB2 phosphorylated at Tyr1248 followed by secondary staining (B). CHO cells were transfected with wild-type ErbB2 followed by fixation, permeabilization and staining with mouse Alexa Fluor 647 secondary antibody (C). The same secondary staining-only procedure was carried out with samples cotransfected with wild-type ErbB2 and EGFR after EGF stimulation. Images recorded in the AlexaFluor647 and GFP channels corresponding to the signal of the secondary antibody and ErbB2-GFP, respectively, as well as differential interference contrast (DIC) images are shown in the figure.

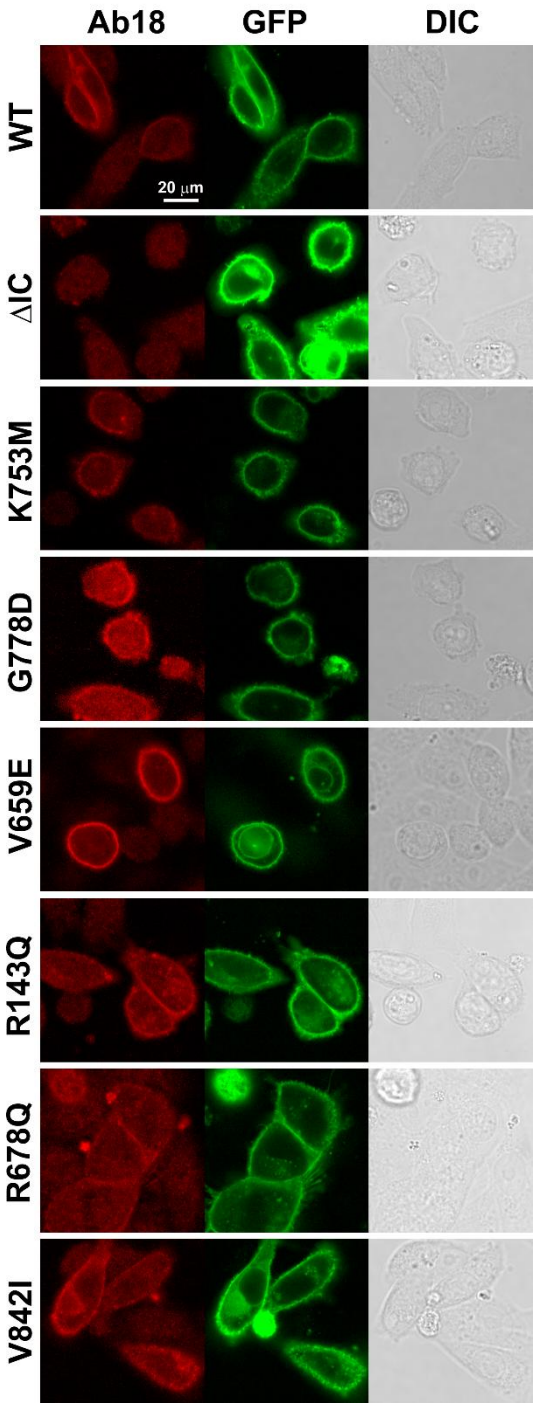

Supplementary Figure 3. ErbB2-specific tyrosine phosphorylation in cells transfected with the ErbB2 variants. CHO cells were transfected with the wild-type or one of the mutant versions of ErbB2. Two days after transfection cells cultured under normal conditions without serum starvation were fixed with 3.7% paraformaldehyde at 4°C for 30 minutes followed by permeabilization with 0.1% Triton X-100 for 10 minutes. The permeabilized cells were labeled with Ab18 against ErbB2 phosphorylated at Tyr1248 followed by secondary labeling with goat anti-mouse Alexa Fluor 647 secondary antibody. The tyrosine phosphorylation signal, the GFP signal corresponding to ErbB2 expression level, and the differential interference contrast (DIC) images are shown in the figure. All images were processed identically to preserve intensity differences.

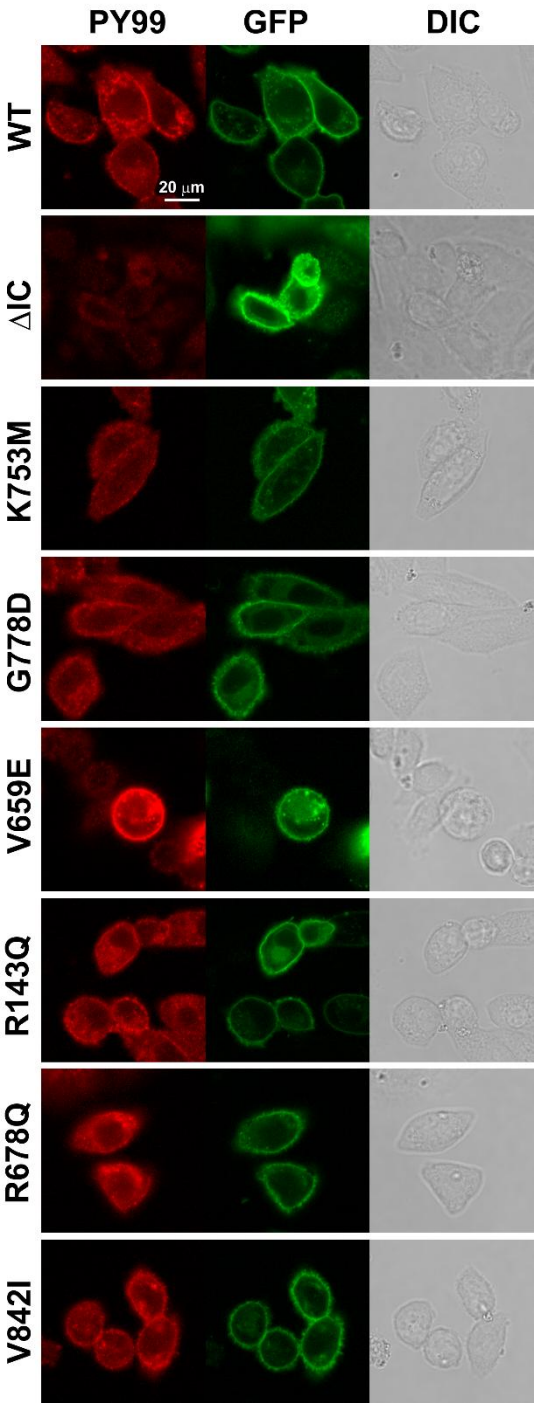

Supplementary Figure 4. General tyrosine phosphorylation in cells transfected with the ErbB2 variants. CHO cells were transfected with the wild-type or one of the mutant versions of ErbB2. Two days after transfection cells cultured under normal conditions without serum starvation were fixed with 3.7% paraformaldehyde at 4°C for 30 minutes followed by permeabilization with 0.1% Triton X-100 for 10 minutes. The permeabilized cells were labeled with PY99 against phosphotyrosine followed by secondary labeling with goat anti-mouse Alexa Fluor 647 secondary antibody. The tyrosine phosphorylation signal, the GFP signal corresponding to ErbB2 expression level, and the differential interference contrast (DIC) images are shown in the figure. All images were processed identically to preserve intensity differences.

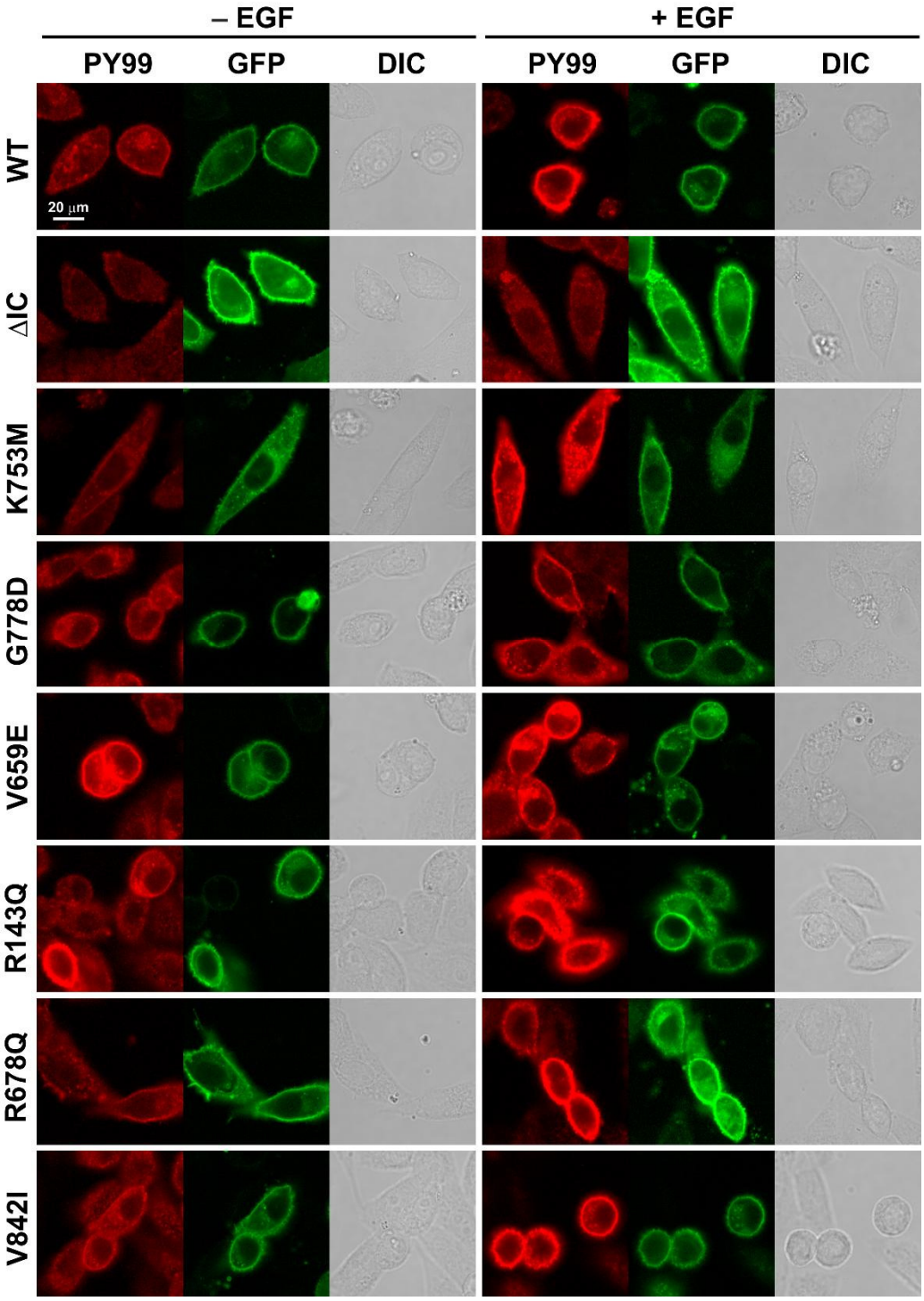

Supplementary Figure 5. Baseline and EGF-stimulated general tyrosine phosphorylation in cells transfected with one of the ErbB2 variants and EGFR. CHO cells were transfected with wild-type EGFR and one of the ErbB2 versions. Beginning one day after transfection, cells were serum-starved overnight followed by stimulation with 50 nM EGF at 37°C for 10 min. Both the stimulated and the control samples were fixed with 3.7% paraformaldehyde at 4°C for 30 minutes followed by permeabilization with 0.1% Triton X-100 for 10 minutes. The permeabilized cells were labeled with PY99 against phosphotyrosine followed by secondary labeling. Images recorded in the GFP channel, showing the GFP fluorescence of the ErbB2 constructs, as well as images showing tyrosine phosphorylation along with the transmission images (DIC) are shown in the figure. All images were processed identically to preserve intensity differences.

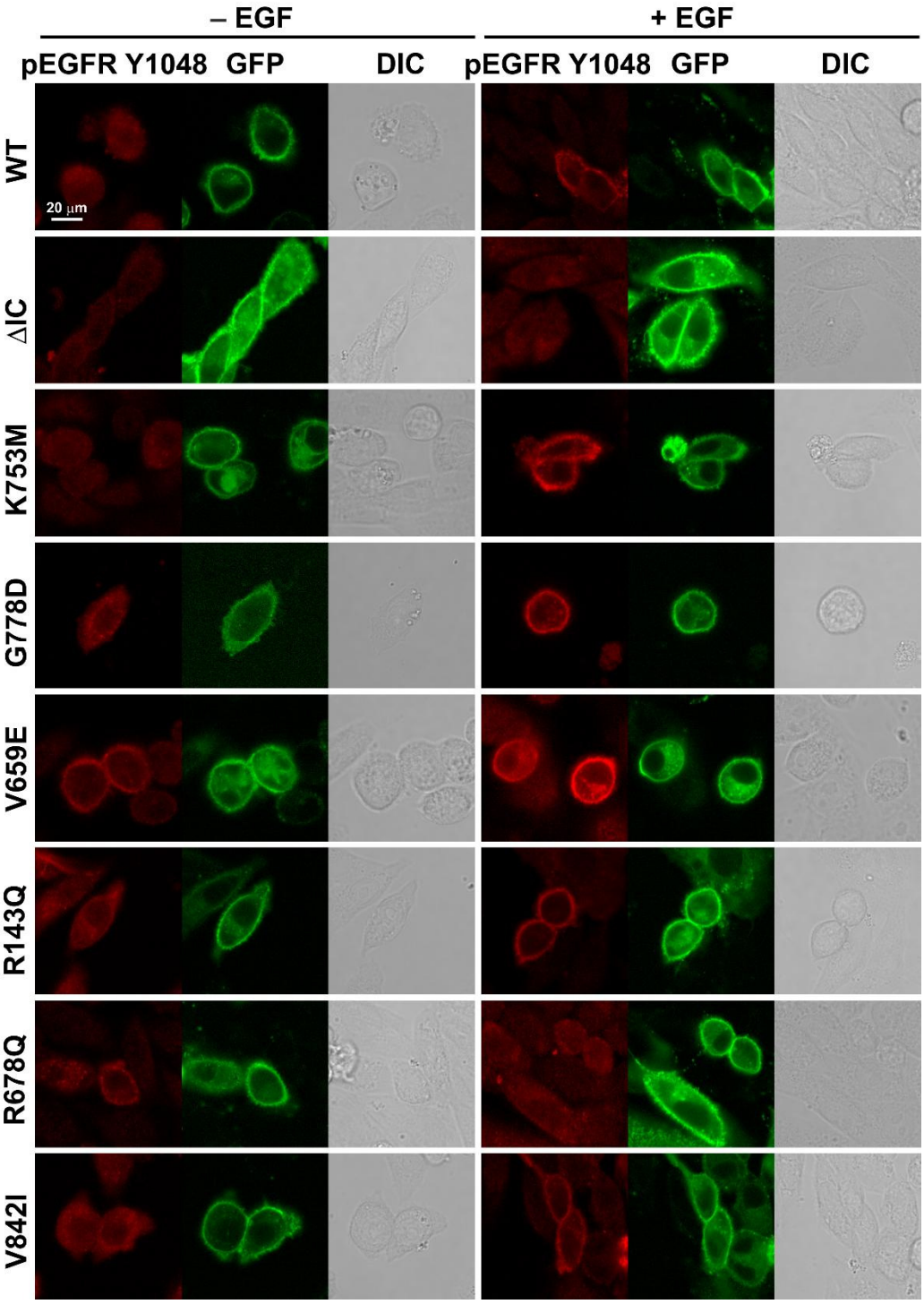

Supplementary Figure 6. Baseline and EGF-stimulated tyrosine phosphorylation of EGFR at tyrosine 1048 in cells transfected with one of the ErbB2 variants and EGFR. CHO cells were transfected with wild-type EGFR and one of the ErbB2 versions. Beginning one day after transfection, cells were serum-starved overnight followed by stimulation with 50 nM EGF at 37°C for 10 min. Both the stimulated and the control samples were fixed with 3.7% paraformaldehyde at 4°C for 30 minutes followed by permeabilization with 0.1% Triton X-100 for 10 minutes. The permeabilized cells were labeled with pEGFR EM-1 Y1048 against EGFR phosphorylated at tyrosine 1048 followed by secondary labeling. Images recorded in the GFP channel, showing the GFP fluorescence of the ErbB2 constructs, as well as images showing EGFR tyrosine phosphorylation along with the transmission images (DIC) are shown in the figure. All images were processed identically to preserve intensity differences.

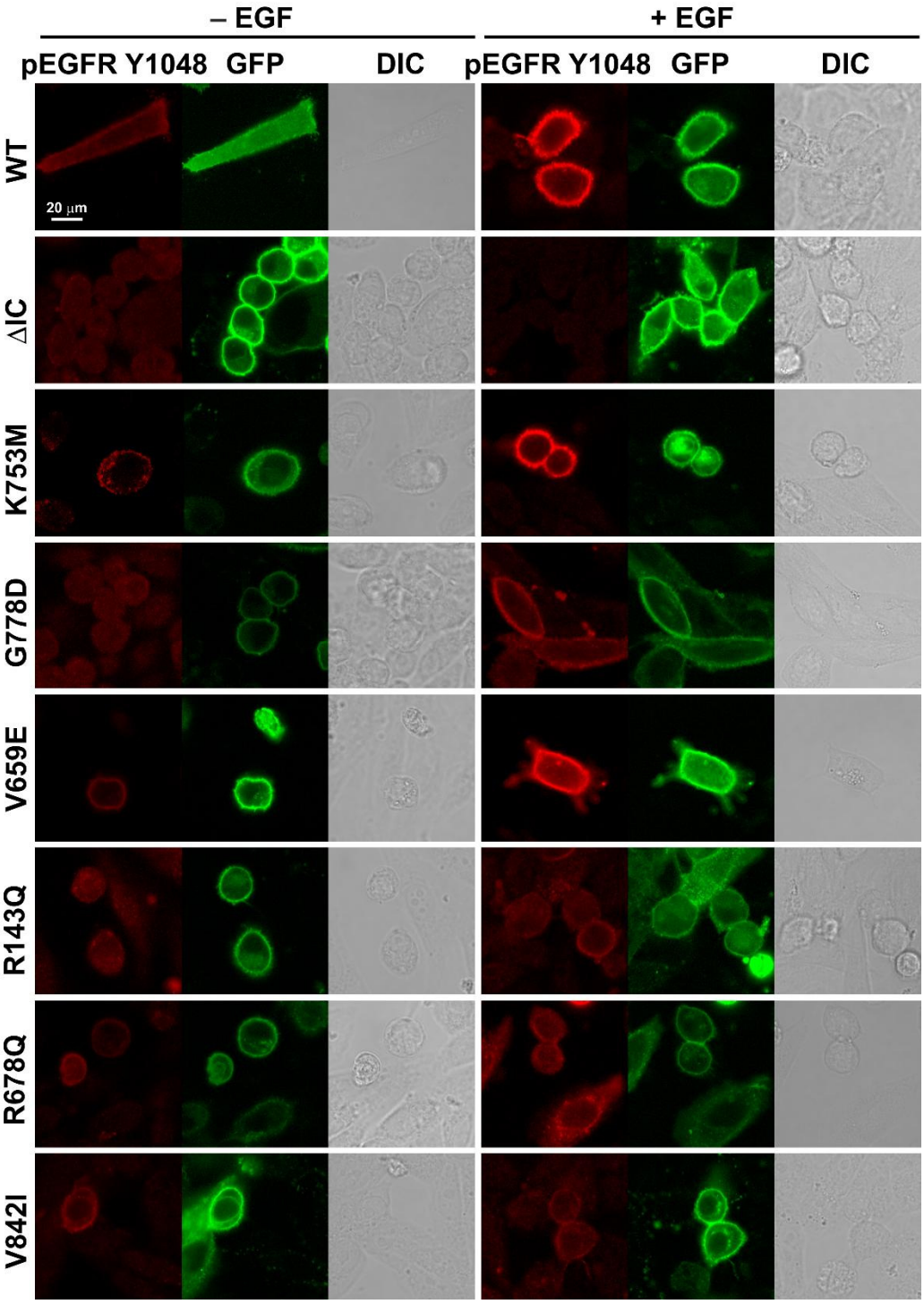

Supplementary Figure 7. Baseline and EGF-stimulated tyrosine phosphorylation of EGFR at tyrosine 1173 in cells transfected with one of the ErbB2 variants and EGFR. CHO cells were transfected with wild-type EGFR and one of the ErbB2 versions. Beginning one day after transfection, cells were serum-starved overnight followed by stimulation with 50 nM EGF at 37°C for 10 min. Both the stimulated and the control samples were fixed with 3.7% paraformaldehyde at 4°C for 30 minutes followed by permeabilization with 0.1% Triton X-100 for 10 minutes. The permeabilized cells were labeled with pEGFR 1H12 Y1173 against EGFR phosphorylated at tyrosine 1173 followed by secondary labeling. Images recorded in the GFP channel, showing the GFP fluorescence of the ErbB2 constructs, as well as images showing EGFR tyrosine phosphorylation along with the transmission images (DIC) are shown in the figure. All images were processed identically to preserve intensity differences.

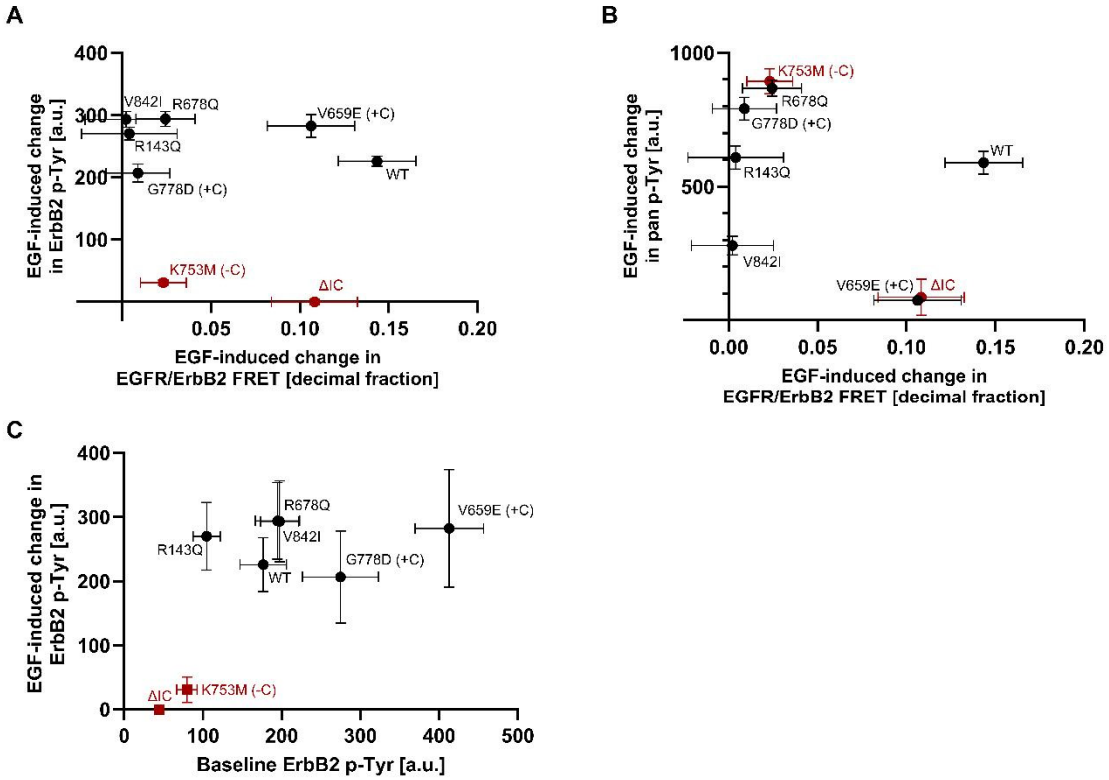

Supplementary Figure 8. Correlation between EGF-induced change in general tyrosine phosphorylation, phosphorylation of ErbB2 at Tyr1248 and ErbB2-EGFR heterodimerization. **(A)** The EGF-dependent increase in ErbB2-specific tyrosine phosphorylation is plotted against the EGF-induced increase in EGFR-ErbB2 heterodimerization, obtained as the difference between FRET in the EGF-treated and control samples in Figure 2C. **(B)** The EGF-dependent increase in general tyrosine phosphorylation is plotted against the EGF-induced increase in EGFR-ErbB2 heterodimerization, obtained as the difference between FRET in the EGF-treated and control samples in Figure 2C. **(C)** Baseline, ErbB2-specific tyrosine phosphorylation and its EGF-induced change, obtained from the data shown in Figure 6B, are plotted against each other. For all panels, the red and black symbols correspond to the active and the inactive versions of ErbB2, respectively. The error bars correspond to the standard error of the mean.